Document downloaded from:

http://hdl.handle.net/10251/156414

This paper must be cited as:

Espinosa-López, JC.; Castro Contreras, R.; Navalón Oltra, S.; Rivera-Cárcamo, C.; Alvaro Rodríguez, MM.; Machado, BF.; Serp, P.... (2019). Influence of Carbon Supports on Palladium Nanoparticle Activity toward Hydrodeoxygenation and Aerobic Oxidation in Biomass Transformations. European Journal of Inorganic Chemistry. (14):1979-1987. https://doi.org/10.1002/ejic.201900190

The final publication is available at

https://doi.org/10.1002/ejic.201900190

Copyright John Wiley & Sons

Additional Information

Influence of carbon supports on palladium nanoparticles activity for hydrodeoxygenation and aerobic oxidation in biomass transformations

Juan C. Espinosa,[a,¥] Ruben Castro Contreras,[b,¥] Sergio Navalón,[a] Camila Rivera-Cárcamo,[b] Mercedes Álvaro,[a] Bruno F. Machado,[c] Philippe Serp,[b]* Hermenegildo Garcia[*,a,d]

[a] Departamento de Química and Instituto de Tecnología Química CSIC-UPV, Universitat Politècnica de València, Consejo Superior de Investigaciones Científicas, Av. de los Naranjos s/n, 46022 Valencia, Spain

[b]*LCC-CNRS, Université de Toulouse, CNRS, INPT, Toulouse, France*

[c]*Laboratory of Separation and Reaction Engineering - Laboratory of Catalysis and Materials (LSRE-LCM), Chemical Engineering Department, Faculty of Engineering, University of Porto, Rua Dr. Roberto Frias s/n, 4200-465 Porto, Portugal*

[d] Center of Excellence for Advanced Materials Research, King Abdulaziz University, Jeddah, Saudi Arabia

[¥] Both are first authors.

Abstract

Three palladium catalysts at similar loadings supported on few-layers graphene, carbon nanotubes (CNT) and carbon nanofibers (CNF) have been prepared by wet impregnation of palladium nitrate. The supports and catalysts have been characterized by chemical analysis, Raman spectroscopy, XRD, electron microscopy and XPS. The average Pd particle size depends on the carbon support, ranging from 1.6 nm for CNF to 2.6 nm for FLG. The catalytic activity of these catalysts was evaluated for two different reactions of interest for biomass transformations, namely hydrodeoxygenation of vanillin to 2-methoxy-4-methyl-phenol that requires a bifunctional catalyst with hydrogenating and Lewis acid sites, and aerobic oxidation of 5-hydroxymethylfurfural to 2,5-furandicarboxylic acid. For the two reactions the activity order of the fresh catalyst was Pd/FLG > Pd/CNF > Pd/CNT, indicating that FLG contributes favorably to the activity in spite of the larger Pd size of the nanoparticles on this support, a fact that has been attributed to the interaction with the prismatic planes on where Pd nanoparticles are located.

1. Introduction

For the sake of sustainability, there is much current interest in developing processes to obtain bulk chemicals from biomass.[1-4] Most of the biomass transformation reactions require catalysts to achieve high conversion and selectivity towards the target product. Since there are numerous reactions in biomass transformations consisting in hydrogenations and aerobic oxidations, many of these processes can be promoted by supported palladium catalysts.[5, 6] Among the preferred supports, carbon derived materials have been widely used due to their availability, large surface area, tunability of surface properties and the ability of these carbon supports to stabilize small Pd nanoparticles (NPs).[7, 8] Since different allotropic forms of carbon have become commercially available, and considering the influence that the support plays on the catalytic activity and stability of supported metal nanoparticles (MNPs), there have been an interest in comparing the performance of these MNPs supported on different carbon nanoforms.[9] In this regard it has been found that carbon nanotubes (CNTs) and few-layers graphenes (FLG) can be used as supports of MNPs due to the interaction between the extended π orbital of the CNT and FLG and the partially empty d orbitals of transition metals.[10-12] In addition, carbon nanofibers (CNFs) consisting in 1D thick carbon materials with long aspect ratio can be advantageous also from the point of view of their availability.[9]

In the present study a series of three Pd catalysts supported on CNT, FLG or CNF has been prepared to evaluate the influence of the support on the palladium catalyst for two different reaction types of interest in biomass transformation, in order to screen their potential applications. Although there are some reports on the activity of other bimetallic catalysts for these reactions,[13] since the focus is on the influence of the carbon supports, the present study

has been focused on Pd nanoparticles that is a metal with general use in the transformation of biomass. Specifically, the reactions under study are shown in Scheme 1. As it can be seen there, one of them is the hydrodeoxygenation of vanillin (V), an abundant starting material,[14, 15] to 2-methoxy-4-methylphenol (MMP). This reaction requires of bifunctional catalyst having hydrogenating activity as well as some acidity.[16] In the literature there are precedents reporting the catalytic hydrodeoxygenation of vanillin using supported noble metal nanoparticles such as Pt, Au and Pd. Of them, Pd was among the most active metals.[17-19] The reported studies support Pd nanoparticles on metal oxides and large area active carbons. However, the possible role of the nature of the carbon support has not been addressed. The second reaction consists in the aerobic oxidation of 5-hydroxymethylfurfural (HMF) to furan dicarboxylic acid (FDCA) that can be a biomass-derived monomer for the preparation of sustainable polyesters.[20-22] HMF is the main platform chemical obtained from cellulose that accounts for 40 % of all the biomass feedstock.[1, 23] Pd containing catalysts have also been used to promote the aerobic oxidation of HMF.[24] The main issue was to achieve high selectivity towards the wanted dicarboxylic acid. Also for this reaction, comparison with other noble metals such as Pt or Au shows the higher activity of Pd.[25] Although active carbon has also been used as support for Pd nanoparticles in HMF oxidation, a detailed study on the influence of different type of carbons has not been made.[26]

a) Hydrodeoxygenation of vanillin

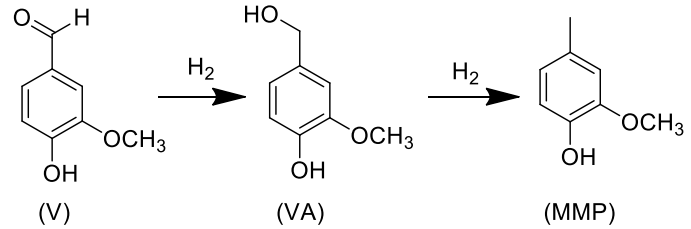

b) Oxidation of 5-hydroxymethylfurfural

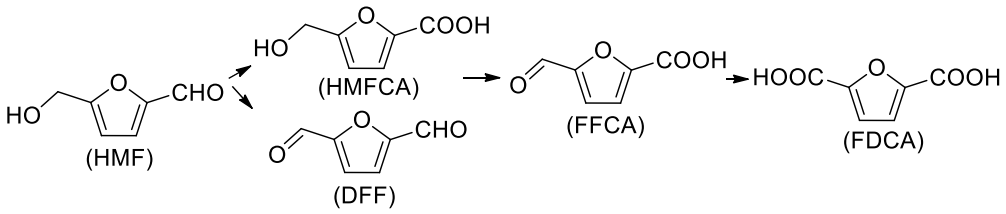

Scheme 1. Two selected biomass transformations that can be catalyzed by Pd NPs supported on carbon materials.

2. Experimental section

2.1. Materials

Vanillin, vanillyl alcohol, 2-methoxy-4-methyl-phenol, 5-(hydroxymethyl)furfural, 5-hydroxymethyl-2-furancarboxylic acid, 5-formyl-2-furoic acid, 2,5-furandicarboxaldehyde, 2,5-furandicarboxylic acid and palladium(II) nitrate dihydrate were supplied by Sigma-Aldrich. Other reagents or solvents employed in the present work were analytical or HPLC grade.

2.2. Materials preparation

CNT_{COOH} syntheses. An $AlCoFeO_4$ catalyst was reduced in a fluidized bed reactor under a nitrogen (225 $mL \cdot min^{-1}$) and hydrogen (150 $mL \cdot min^{-1}$) flow at 650 °C. After the reduction step, the ethylene flow was adjusted to 225 $mL \cdot min^{-1}$ for 30 min to produce CNT. The CNT were recovered and then purified using an aqueous solution (50 vol% H_2SO_4) under reflux at 140 °C for 3 h. The acidic solution was then filtered and the solid washed with distilled water. The resulting solid was dried in an oven at 80 °C overnight. The purified CNT was then functionalized with HNO_3 under reflux at 140 °C for 3 h. The acidic solution was filtered and washed with distilled water. The resulting solid was dried in an oven at 80 °C overnight to produce functionalized CNT (CNT_{COOH}).

FLG_{COOH} syntheses. A $CoFe_2O_4$ catalyst was reduced in a fluidized bed reactor under a nitrogen (225 $mL \cdot min^{-1}$) and hydrogen (150 $mL \cdot min^{-1}$) flow at 650 °C. After reduction step, the ethylene flow was adjusted to 225 $mL \cdot min^{-1}$ for 30 min to produce FLG. The FLG was recovered and purified at room temperature overnight using HCl. The acidic solution was then filtered and washed. The resulting solid was dried in an oven at 80 °C overnight. The

purified FLG was then functionalized with HNO_3 under reflux at 140 °C for 3 h. The acidic solution was filtered and washed. The resulting solid was dried in an oven at 80 °C overnight to produce functionalized FLG (FLG_{COOH}).

CNF_{COOH} syntheses. A $CoFe_2O_4$ catalyst was reduced in a fluidized bed reactor under a nitrogen (225 $mL \cdot min^{-1}$) and hydrogen (150 $mL.min^{-1}$) flow at 450 °C. After the reduction step, the ethylene flow was adjusted to 225 $mL \cdot min^{-1}$ for 30 min to produce CNF. The CNF were recovered and then purified at room temperature overnight using HCl. The acidic solution was then filtered and washed. The resulting solid was dried in an oven at 80 °C overnight. The purified CNF was functionalized using HNO_3 under reflux at 80 °C for 3 h. The acidic solution was then filtered and washed. The resulting solid was dried in an oven at 80 °C overnight to produce functionalized CNF (CNF_{COOH}).

Pd/carbon nanomaterials. A wet impregnation method was used to prepare the palladium catalysts supported on carbon nanomaterials. The desired amount of $Pd(NO_3)_2 \cdot 2H_2O$ was added to an acetone solution (100 mL) containing 1 g of carbon nanomaterial, so as to introduce 2 w/w% of metal phase. The solution was then sonicated at room temperature for 1 h and magnetically stirred overnight. The solution was then filtered and washed with acetone that ensures that only strongly bond Pd^{2+} remains on the support. The main factors responsible for Pd loading are specific surface area and surface acidity of the carbon materials.[27-29] The resulting solid was dried in an oven at 120 °C overnight. Finally, the catalyst was reduced in a horizontal tube oven under a nitrogen and hydrogen flow (20 vol% H_2) at 300 °C for 2 h.

2.3. Materials characterization

TEM micrographs were taken with a JEOL JEM 1011 microscope operating at 100 kV. Palladium particle size distribution was calculated using the ImageJ software measuring at least 250 particles. XRD patterns were recorded at room temperature with a Panalytical X'PERT PRO diffractometer, employing a Cu-Kα radiation (λ = 1.54 Å) and a parabolic MPD-mirror for Cu radiation. The diffractograms were acquired in 2θ range of 5−90°, using a continuous scan mode with an acquisition step size of 0.0170° and a counting time of 299.72 s. Raman spectra were measured in a micro Raman Spectrometer HR 800 Jobin Yvon Horiba using a laser of 532 nm wavelength as excitation source. Nitrogen adsorption measurements were performed at −196 °C using a 3Flex Surface Characterization Analyzer (Micromeritics GmbH). The surface area was measured using Brunauer, Emmet and Teller (BET) method. The pore radius distribution was determined by the Barrett, Joyner and Halenda (BJH) method. Before analysis, the samples were degassed at 150 °C using a Micromeritics VacPrep 061 Sample Degas System until a static pressure of less than 0.01 Torr (0.0133 mbar) was reached. The elemental results were obtained using a CHN Perkin-Elmer elemental analyzer. Palladium loadings were determined using an iCAP 6300 ICP Spectrometer, by digestion of the samples in hot aqua regia. The adsorptive potential distributions were calculated from the adsorption isotherms using the standard software implemented in the apparatus (3Flex Version 4.04). The calculation of the DFT, basal plane and "non-basal plane" surfaces as well as of the respective ratios has been performed as previously described.[30] The surface chemical composition of the carbon materials was analyzed by XPS (Kratos AXIS Ultra HSA spectrometer), using a Mg-Kα radiation (1486.7 eV). The existing elements, and their corresponding concentrations, were determined by

recording a survey spectra up to a binding energy (BE) of 1300 eV. High-resolution XPS spectra of the C1s, and Pd3d core levels and full-width-at-half-maximum (FWHM) values were used to assess the chemical state of these elements at the catalyst surface, according to the NIST database. Inductively coupled plasma-atomic emission spectroscopy (ICP-AES) was employed to determine the amount of possible Pd leaching from the catalyst to the solution upon reaction.

2.4. Catalytic tests

Hydrodeoxygenation of vanillin was carried out in a pressurized glass reactor. Briefly, vanillin (40 mg) dissolved in H_2O (2 mL) was placed together with the required amount of catalyst (i.e. 10 mg). The mixture was sonicated in an ultrasound bath (450 W) for 30 min to ensure a good dispersion of the catalyst. Then, the reactor was purged five times with H_2 and, then, pressurized at 5 bar. The system, under stirring, was heated at 100 ºC employing a preheated oil bath. This event was considered the 0 reaction times. At the required times, aliquots were taken from the reactor (100 µL), diluted with H_2O (100 mL) and filtered (0.2 µm Nylon filter) before analysis by HPLC.

The oxidation of HMF was carried out in a pressurized glass reactor. HMF (19 mg) was dissolved in H_2O (2 mL) containing K_2CO_3 as base (42 mg) and, then, the required amount of catalyst was added (i.e. 10 mg). The mixture was sonicated for 30 min with a power of 450 W. This relatively low sonication power ensures good dispersion of the catalyst in the reaction mixture without producing structural changes. The reactor was purged with oxygen five times and pressurized with oxygen (5 bar) before heating the system at 160 ºC, under stirring, in a preheated oil batch. The initial reaction rate was considered when the reactor was introduced into the bath.

Reusability experiments for each reaction were carried out under the corresponding conditions indicated above. At the end of the reaction the catalyst was recovered by filtration employing a nylon membrane (0.2 µm). The used catalyst was thoroughly washed with water and ethanol and, then, dried in an oven at 100 °C. The resulting solid was employed in a subsequent catalytic cycle. This procedure was repeated three times.

The heterogeneity of the reaction was tested by performing the hot filtration test. This test consists in removing the catalyst from the reaction mixture after depressurization filtering the suspension without cooling (~80 ºC) at the reaction temperature at a certain conversion. The hot filtrate was allowed to react further, in the absence of solid, under the reaction conditions.

2.5. Analysis of the reaction. The reagents and products of both reactions under study (Scheme 1) were analyzed by HPLC using a photodiode array as detector. Previously filtered reaction aliquots were injected in the HPLC system equipped with a reverse-phase chromatography column (Kromasil-CN for vanillin (V) reaction or Kromasil-C18 for HMF reaction) as stationary phase. Mobile phase working under isocratic conditions for compounds V and HMF were H_2O:CH_3CN (40:60 vol%) or H_2O, respectively.

3. Results and discussion

3.1. Catalyst support and catalyst characterization

Three kinds of carbon materials presenting different arrangement of the graphene layers, CNTs, CNFs, and FLG were used as support for palladium deposition. CNT, CNF and FLG supports were previously oxidized with nitric acid to increase the concentration of surface carboxylic groups, which should act as anchoring sites for MNPs.[31] The elemental analysis, XPS and XRD patterns, and nitrogen adsorption data of these three supports are listed in Table 1. TEM micrographs of the supports are provided in Figure S1.

Table 1. Chemical, textural, and crystallite parameters of the carbon supports used in the present study.

Supports	Elemental analysis	XPS analysis		Textural properties		Crystallite parameters		
	C (%)	C (%)	O (%)	BET surface area ($m^2.g^{-1}$)	Pore volume ($cm^3.g^{-1}$)	d_{002} (nm)	$L_C(002)$ (nm)	$L_a(110)$ (nm)
CNT_{COOH}	90.4	94.3	5.7	220	1.2	0.3407	4.48	7.95
FLG_{COOH}	97.1	96.2	3.8	51	0.2	0.3393	10.34	16.05
CNF_{COOH}	95.7	93.4	6.6	71	0.3	0.3434	4.64	10.95

These materials show different arrangements of the graphene layers. Among the filamentous carbon materials, we can distinguish between CNTs, for which the graphene layers are parallel to the filament axis, and CNFs, for which an angle exists between the filament axis and the graphene layers. The average angle with respect to the filament long axis is ~26° for CNF. For this latter support, disordered amorphous carbon can be occasionally observed at its surface, resulting in a mixture of edges and disordered carbon (Figure S2). The mean external diameter of CNFs is 50 nm, and their mean inner diameter is 6 nm. The CNTs are multi-walled, with an average external diameter of 15 nm, and an internal diameter of 7 nm. They are composed of 5-10 graphene layers. The FLG consists in graphitic flakes of turbostratic carbon of around 1 μm^2 the number of graphene layers ranges between 5 and 50. The elemental analysis shows a high level of purity for these materials (90-97%). The treatment with nitric acid, for a given type of material, results in an increase of the amount of surface oxygen, as revealed by XPS. The percentage of oxygen determined by XPS for the purified supports was: 0.8 for CNTs, 0.9 for FLG and 1.5 for CNFs. The textural properties of the supports have been evaluated from nitrogen adsorption/desorption isotherms. These carbon materials present pore volumes of 0.2 to 1.2 $cm^3 \cdot g^{-1}$ and are predominantly mesoporous. For the filamentous carbons, the pores arise from interstices between entangled fibers or tubes. The specific surface area of the supports ranged between 50 and 220 $m^2 \cdot g^{-1}$. Type IV isotherms with type H_2 hysteresis loops were obtained (Figure S3), suggesting that the supports are mainly mesoporous and contain, as expected, a small number of micropores. Since the ratio between the basal plane and "non-basal plane" surface areas should be an important factor in determining the surface reactivity of these materials, DFT calculations, derived from nitrogen adsorption data, were used for the determination of

surface heterogeneities in these supports by adsorptive potential distribution.[32] Thus, the absolute and relative proportion of basal plane and "non-basal plane" surface areas can be determined from the nitrogen adsorption measurement, followed by an evaluation of the adsorption data using DFT.[30] The "non-basal plane surfaces" can be further subdivided into prismatic surfaces and "defect surfaces" (the latter contain surface groups and other surface defects). Figure 1 depicts the percentages of prismatic: basal: defect surfaces. The highest proportion of basal surface area is observed for CNTs, followed by FLG. The fact that the produced FLG flakes present a significant number of layers (5-50) and defect density (see Raman spectra) could explain this result. As expected, CNF presents a significant amount of defects. This should be related to the surface of the CNF being composed of a mixture of edges and disordered carbon, as already discussed (Figure S2). From this characterization, we can anticipated that the CNF support with high proportion of edges and defects should not favour metal sintering due to a limited metal diffusion on such a surface.

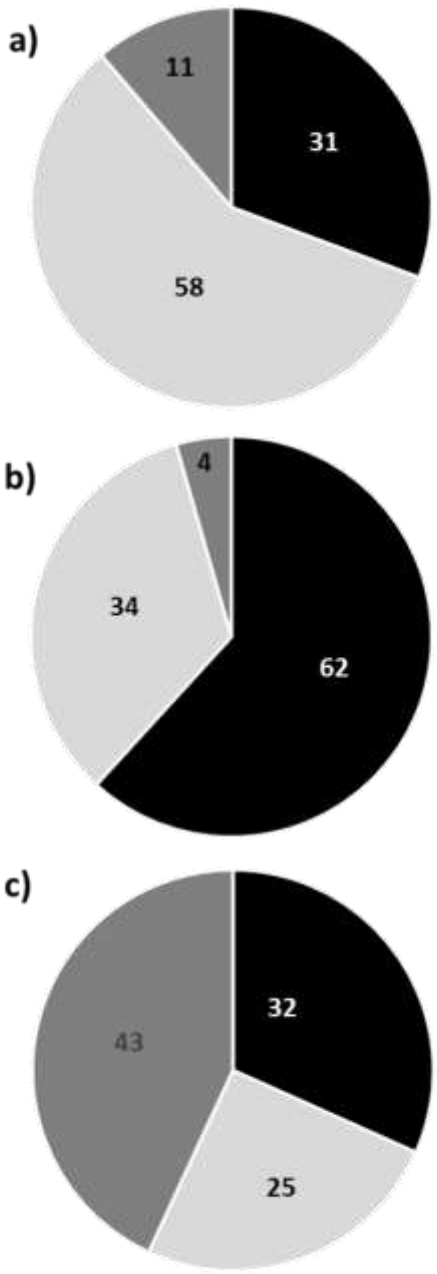

Figure 1. Percentage of prismatic (black) : basal (light grey) : defect surfaces (dark grey) surface area of the supports. a) CNT; b) FLG, and c) CNF.

The d_{002} graphene interlayer distances, the average crystallite size considering the particles as parallelepiped in the basal plane (parallel to the hexagonal layers, L_a) and parallelepiped height (perpendicular to the hexagonal layers, L_c). These parameters were determined from the position of the corresponding peaks in XRD.[33] The corresponding diffractograms are given in Figure S4. The highest intensity for the graphite (002) peak ($2\theta = 26°$) and therefore d_{002} values close to the value for graphite (0.335 nm), was observed for the FLG support. This support shows also the largest crystallite size.

The Raman and detailed XPS characterizations of the carbon supports are reported in Table 2. The best fit for the main C1s spectrum (Figure S5) was obtained by deconvoluting the experimental high resolution XPS peak into seven line shapes: i) peak i, at around 283.7 eV, is attributed to the presence of point defects (C vacancies, pentagon and heptagon rings, Stone-Wales defects); ii) peak ii, at 284.6 eV, represents sp^2 C−C bonds; iii) peak iii, at 285.1-285.2 eV, is assigned to sp^3 carbon species; iv-vi) the peaks at 286.0-286.2 (iv), 287.3-287.5 (v), and 288.4-289.2 eV (vi), correspond to carbon atoms attached to different oxygen-containing groups; and vii) the π–π^* transition loss peak is detected at 290.6-291.2 eV.[34-36] For all the investigated supports, significant amounts of oxygenated species were detected (peaks iv, v and vi in XPS C1s peak), resulting from HNO_3 oxidation. The amount of sp^3 carbon follows the order CNF > CNT > FLG. The amount of sp^2 carbon follows the opposite order. FWHM of the C 1s peak has been used to assess the graphitic nature of the supports, with a larger FWHM corresponding to a more disordered structure.[37]

Raman spectroscopy was also used to evaluate the degree of structural order of the supports. It provides analogous information to XRD, although it has the advantage of surface specificity, thus allowing the study of very heterogeneous materials. The most important

parameter calculated Raman spectroscopy is the ratio between the integrated intensities of the D band (I_D) at ~1380 cm^{-1}, attributed to the defects of the graphitic structure, and G band (I_G) at ~1580 cm^{-1}, which is ascribed to a graphitic (ordered) structure, both bands belonging to the first-order Raman spectrum for carbon materials. Another parameter, measurable by Raman spectroscopy, which is relevant to catalyst preparation, is the L_D; L_D is a typical inter-defect distance, with the defect being considered a point-like (zero-dimensional) structure.[38] A quantification of the long-range order in the support can also be made from the graphitic in-plane microcrystallite size, L_a.[39] The Raman analyses confirm the XPS results in the sense that both analyses point to a higher order in FLG: low I_D/I_G, large L_a and L_D, and narrow FWHM. The most defective support is CNF, and CNT constitutes an intermediate situation.

Table 2. Raman analyses (intensity ratio of the Raman G and D bands (I_D/I_C) and inter-defect distance (L_D) and microcrystallite size (L_a)) and XPS C1s peak components of the carbon supports employed in the present study.

Supports	Raman analysis			XPS analysis C1s peak							
	I_D/I_G	L_D (nm)	L_a (nm)	FWHM (eV)	i	ii	iii	iv	v	vi	vii
CNT_{COOH}	1.01	11.9	19	0.72	1.3	56.6	9.8	10.0	7.0	5.6	9.6
FLG_{COOH}	0.64	15.0	30	0.69	0.9	62.1	7.0	9.6	6.0	5.1	9.3
CNF_{COOH}	1.24	10.7	15	0.76	4.6	52.1	10.5	10.4	7.2	6.3	9.0

From all these analyses, some conclusions can be drawn regarding palladium catalyst preparation and use. Firstly, if we consider the prismatic: basal : defect surfaces of the supports, the palladium-carbon support interface/interaction should be different for these catalysts. It is expected to have a higher proportion of Pd-prismatic surface interaction for FLG, and a higher proportion of Pd-defect surface interaction for CNF. CNTs constituting an intermediate situation. Secondly, considering the surface area of the supports, and the long range order according to Raman, XRD and XPS analyses, it can be anticipated that palladium surface migration, and thus possible sintering should be favoured on FLG. On CNFs, the presence of disordered carbon on their surface should limit this unwanted agglomeration. Finally, considering the high proportion of oxygenated surface species, the palladium dispersion should be relatively high for the three supports.

The 2 w/w% Pd catalysts were prepared by wet impregnation using hydrated Pd nitrate. This precursor was chosen because its reduction yields impurity-free Pd particles. Table 3 shows the characterization data for the Pd catalysts. The specific surface area of the catalysts did not change significantly compared to the bare supports. XRD analyses show a very small and broad Pd(111) peak at $2\theta = 40.1\ ^{o}$ characteristic of metallic palladium (Figure S6), pointing to a small Pd particle size. The palladium particle size was measured from TEM micrographs, and the metal dispersion was calculated from an equation for metal dispersion from TEM, assuming a spherical particle geometry, as described elsewhere.[40] Representative micrographs, and particle size distributions are shown in Figure 2. It is worth mentioning that for CNTs that present an inner cavity, some particles should be located in this cavity. The higher palladium dispersion was obtained on CNFs, presumably because of a higher concentration in surface oxygenated species (Table 1), and a higher concentration of defects

(XRD, Raman, and XPS analyses). Similar dispersion were obtained on CNTs and FLG. This results might appear surprising, considering the fact that CNTs have a larger surface area (220 $m^2 \cdot g^{-1}$) compared to FLG (50 $m^2 \cdot g^{-1}$), and larger amount of surface oxygen groups (Table 1). We propose that this result arises from the surface on which these MNPs are deposited: mainly prismatic surface for FLG, and basal surface for CNTs. Figure 2b clearly shows that Pd NPs are preferentially deposited on the edges of the FLG support.

Table 3. Metal loading, surface area, Pd mean size and dispersion for the investigated catalysts.

	Pd (%)	BET surface area ($m^2.g^{-1}$)	Particle size (nm)[a)]	Pd dispersion (%)
Pd/CNT_{COOH}	2.04	232	2.2 ± 1.1	49
Pd/FLG_{COOH}	1.87	50	2.6 ± 1.6	43
Pd/CNF_{COOH}	1.70	82	1.6 ± 0.9	67

a) From TEM.

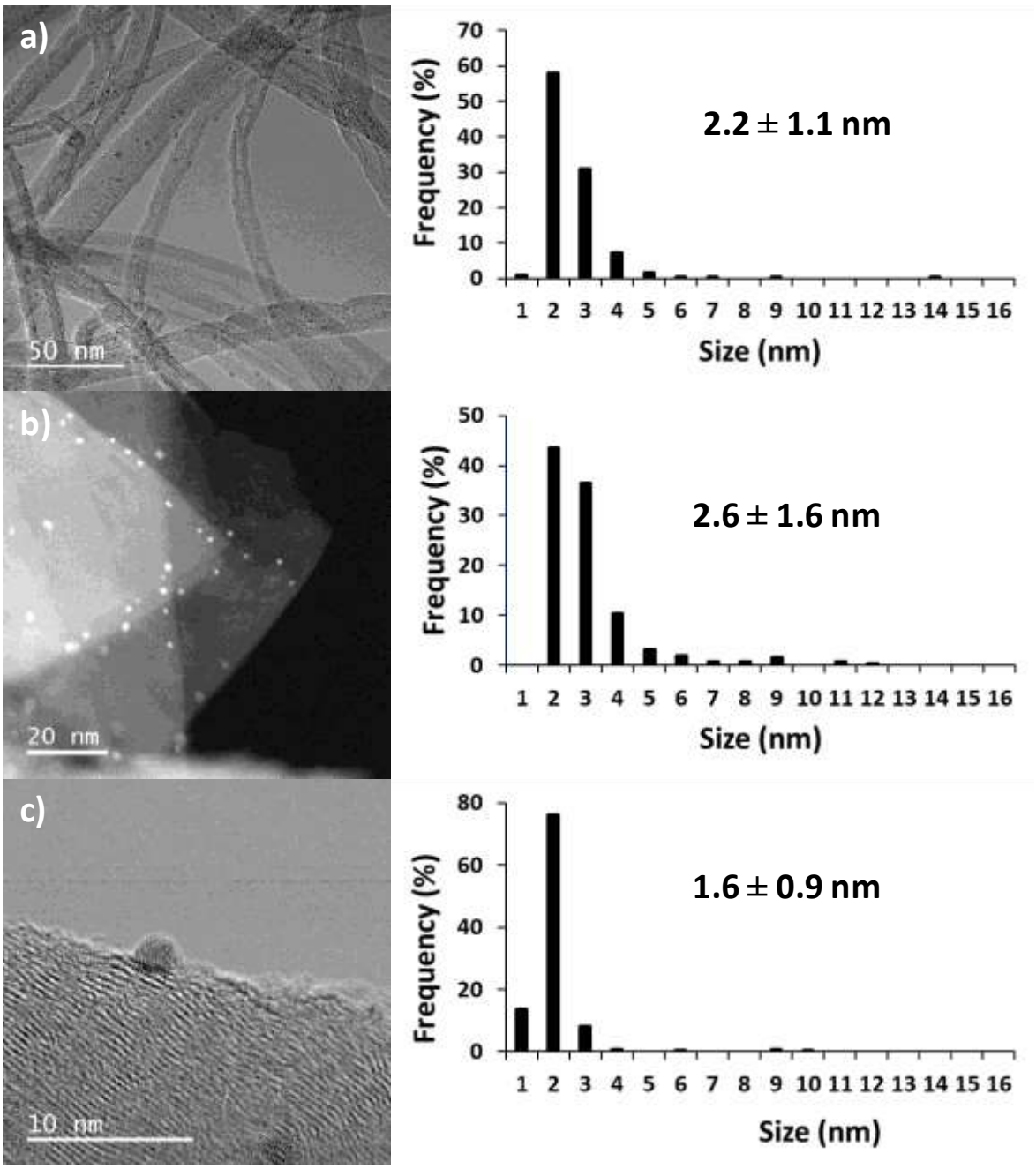

Figure 2. Representative micrographs and particle size distribution for: a) Pd/CNT – HRTEM (scale bar = 50 nm); b) Pd/FLG – STEM-HAADF (scale bar = 20 nm); and c) Pd/CNF – HRTEM (scale bar = 10 nm).

The catalysts have also been analyzed by XPS (Figure S7 and Table 4). The XPS Pd 3d peak for all catalysts was wide, indicating either multiple oxidation states of the Pd species, or several different interactions of the oxidized carbon support. Peaks at 335.5 and 340.5 eV, were assigned to Pd(0) $3d_{5/2}$ and $3d_{3/2}$, respectively, while the $3d_{5/2}$ and $3d_{3/2}$ peaks for Pd^{2+} are at 337.8 eV and 343.4 eV. The XP spectra of palladium catalyst showed peaks for Pd $3d_{5/2}$ and Pd $3d_{3/2}$ with Pd(0) and Pd^{2+} combined lines, but Pd^{2+} line as dominant. The presence of higher Pd oxidation states are indicated by the Pd $3d_{5/2}$ peak at a binding energy of 339 eV, which can be assigned to PdO_2 or $Pd(OH)_4$. From the deconvolution pf the XPS Pd 3d peak it appears that, while Pd/CNT and Pd/FLG have a similar distribution of Pd^0 vs. oxidized Pd atoms, Pd/CNF has a larger population of reduced Pd^0.

Table 4. XPS Pd 3d peak components and the ratios between reduced and oxidized Pd atoms for each catalyst.

Catalyst		XPS analysis Pd 3d peak						
	i	ii	iii	iv	v	vi	Pd^0/Pd^{2+}	Pd^0/Pd_{ox}
Pd/CNT_{COOH}	12.30	8.18	39.92	26.54	7.85	5.22	0.31	0.26
Pd/FLG_{COOH}	12.30	8.18	39.44	26.22	8.33	5.53	0.31	0.26
Pd/CNF_{COOH}	18.01	11.97	38.37	25.50	3.70	2.46	0.47	0.43

3.2. Catalytic reactions

The three supported Pd catalysts were used as catalysts for the two processes of relevance in biomass transformation indicated in Scheme 1. As commented in the introduction one of the reactions under study was the hydrodeoxygenation of vanillin (V) to 2-methoxy-4-methylphenol (MMP). This transformation encompasses two consecutive steps, the first one being hydrogenation of conjugated aldehyde group to a benzylic alcohol requiring hydrogenation sites followed by hydrodeoxygenation of the hydroxyl group by acid sites. Both steps, hydrogenation of carbonyl groups and removal of oxygen are very common in biomass transformation by bifunctional catalysts and, therefore, the results achieved for the transformation of vanillin to MMP with the different Pd catalysts should also be readily expanded to many other hydrogenations and hydrodeoxygenations. The reaction was carried out under moderate hydrogen pressure (5 bar) in water as solvent at the boiling temperature in the presence of the three Pd-catalysts under study.

The only product observed in the process as reaction intermediate is vanillyl alcohol (VA). Figure 3 shows the temporal evolution of vanillin conversion as well as the yields of vanillyl alcohol (VA) intermediate and the wanted 2-methoxy-4-methylphenol (MMP). As it can be seen in this Figure 3, even though the palladium content is similar for the three materials, the solids exhibit contrasting catalytic activity. The order of activity based on conversion of V being Pd-FLG > Pd-CNF > Pd-CNTs. Besides conversion of V, subsequent disappearance of vanillyl alcohol and MMP also follows the same order as the disappearance of vanillin. While the relative activity of Pd/CNF versus Pd/CNT can be explained based the smaller particle size of Pd NPs in Pd/CNF compared with Pd/CNT, the high activity of Pd/FLG cannot be predicted based on Pd particle size that is higher in Pd/FLG compared to the other two catalysts. Also, Pd dispersion on FLG is lower than for the other two carbon

supports. Thus, other properties of FLG as support and, particularly, the presence of prismatic planes on which the Pd NPs are interacting with the support should be playing a role determining Pd catalytic activity. Thus, considering that Pd NPs are the active sites and carbon supports play a major role interacting with those Pd NPs, it is proposed that the main factor responsible for the higher activity of Pd/FLG respect to the other two catalysts would be the specific location of the Pd NPs on the prismatic planes present on FLG.

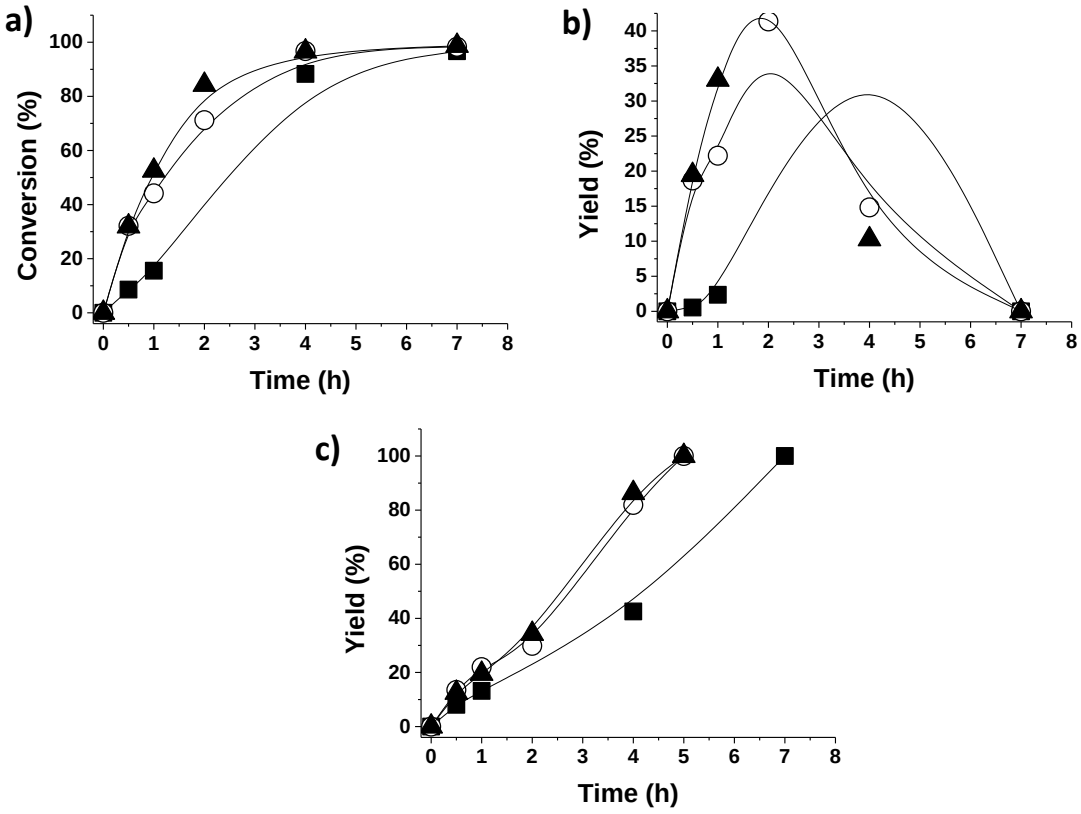

Figure 3. Vanillin conversion (a), vanillyl alcohol evolution (b) and 2-methoxy-4-methylphenol (c) formation using Pd/CNT (■), Pd/CNF (○) and Pd/FLG (▲) as catalysts. Reaction conditions: Catalyst (10 mg), vanillin (20 g L^{-1}; 0.13 M), 2 mL H_2O, 5 bar H_2, 100 °C.

Stability of carbon-supported Pd catalysts was studied by performing a series of reuses of vanillin (V) to 2-methoxy-4-methylphenol (MMP). The results are presented in Figure 4 and S8-S9 in the supporting information. As it can be seen in these Figures, one of the most surprising results was that although the temporal profiles of three consecutive for vanillin disappearance using Pd/FLG as catalyst were coincident indicating that the catalytic activity for hydrogenation of V into VA is maintained, the rate of the second step of hydrodeoxygenation decreases considerably upon reuse, particularly from the fresh to the first used catalyst. Although, as it can be seen in Table 5, a slight growth of the average Pd NP size was observed for the three supported Pd, the size increase was about 1 nm. Thus, it seems that this decay in activity cannot be attributed to the minor changes in the Pd NP size distribution. Therefore, other causes have to be invoked to explain catalytic activity decay.

Since it seems that it the second hydrodeoxygenation step is the one limiting the overall conversion of V into MMP, it could be that Pd/FLG becomes deactivated due to the strong adsorption of the aromatic intermediate VA or MMP. To support this possibility, the TPD profile of the used Pd/FLG catalyst after exhaustive washings was performed and compared to that of the fresh Pd/FLG sample. The results are presented in Figure S10 confirming that the spent Pd/FLG catalyst desorbs in the range of temperature from 250 to 700 °C considerably a larger amount of adsorbed reaction intermediates that are absent in the fresh catalysts. However, control experiments performing the reaction under the general conditions but adding on purpose at initial reaction time 30% of VA or MMP did not show sign of catalyst deactivation in the temporal profile of vanillin conversion or intermediates evolution. These experiments rules out VA or MMP as catalyst poison. It is proposed that other byproducts could be the responsible for this deactivation. This proposal is somehow

supported by comparison of the composition by elemental analysis of the three palladium catalysts, fresh or after the reaction (see table S1 in the supporting information). While in the cases of Pd/CNT and Pd/CNF the differences in the carbon and hydrogen between the fresh and used materials are not relevant, for Pd/FLG a decrease in the carbon content of about 5% upon catalyst use was measure suggesting that this material has adsorbed reaction intermediates, products or substrates during the reaction. Therefore, it seems that deactivation in the case of Pd/FLG occurs by strong adsorption of products and intermediates.

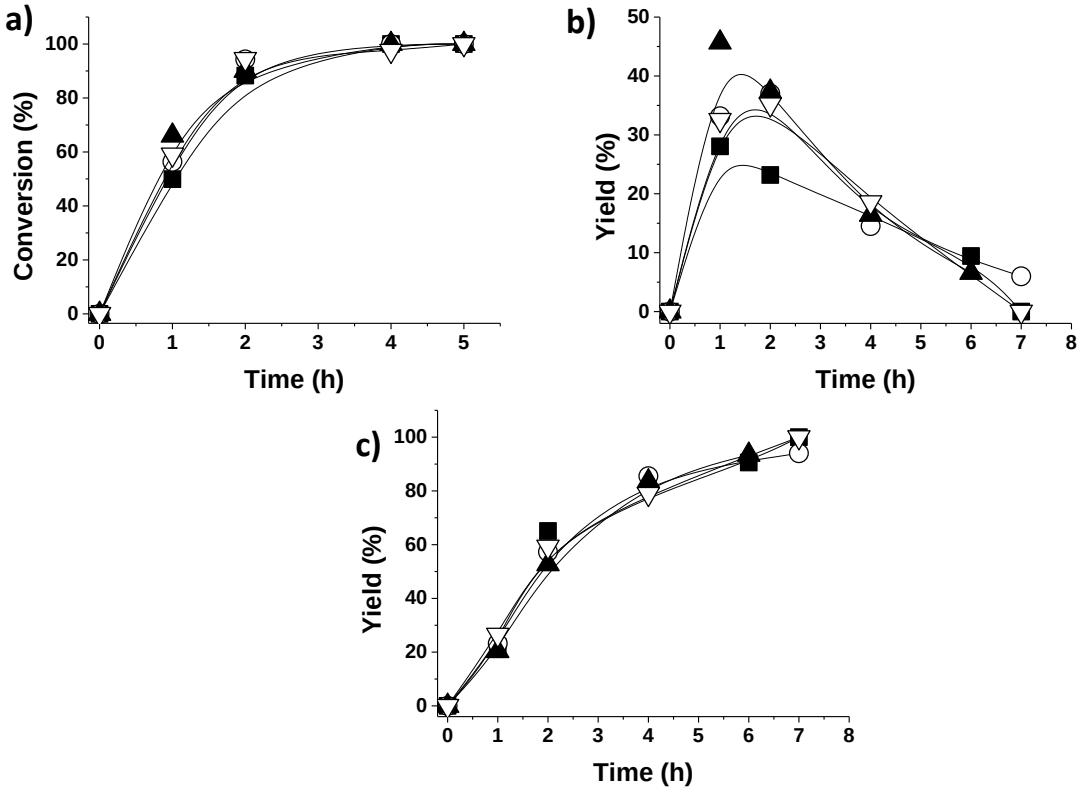

Figure 4. Vanillin conversion (a), vanillyl alcohol evolution (b) and 2-methoxy-4-methylphenol (c) formation using Pd/CNF as catalyst during four consecutive uses. Legend: First use (■), second use (○), third use (▲) and fourth use (▽). Reaction conditions: Catalyst (10 mg), vanillin (20 g L^{-1}; 0.13 M), 2 mL H_2O, 5 bar H_2, 100 °C.

In contrast to Pd/FLG, Pd/CNT and, particularly, Pd/CNF (compare Figures 4 with S8 and S9), although the fresh materials are initially less active, both, Pd/CNT and Pd/CNF, maintain a significant degree of catalytic activity in the two steps, indicating their higher stability under the reaction conditions. In this regard, Pd/CNF combines both a reasonable catalytic activity and a notably high reusability. Chemical analysis of the liquid phase after removal of the solid Pd/CNF catalyst showed that the Pd content in the liquid was only about 0.1 wt% of the initial supported palladium content, indicating the heterogeneous nature of the catalytic process. Higher palladium leaching was observed when using the Pd/CNT (0.3 wt%) sample and, particularly, when using Pd/FLG (2.3 wt%). Heterogeneity of hydrodeoxygenation of vanillin to MMP was also supported by performing a hot filtration test in which the reaction was carried out in the presence of Pd/CNF solid under the general reaction conditions and, then, the catalyst was filtered after depressurization of the reaction mixture while the mixture was still hot (~80 ºC) at 30 % conversion, observing that the reaction completely stops in the absence of catalyst (Figures S11a-c).

The second reaction under study was the aerobic oxidation of HMF to 2,5-furandicarboxylic acid (FDCA) using molecular oxygen under pressure. This oxidation generally requires the presence of base in order to take place, although there are scattered examples in where bases are not needed. A control experiment in the present case using Pd/FLG in the absence of base for the oxidation of HMF was unsuccessful, meaning that bases are needed under the present reaction conditions. After a series of preliminary trials, K_2CO_3 was found a convenient base for the process in our case. The role of the base is to promote the formation of alcoholate that should bind to the surface of Pd NPs stronger than the corresponding alcohol. The reaction is carried out in water as solvent at 160 ºC. During

the course of the reaction hydroxymethylfuroic acid (HMFCA) was observed as the major reaction intermediate, accompanied by lesser proportions of the corresponding aldehydes DFF and FFCA. A summary of the results is presented in Figure 5, where the relative activity order can also be inferred.

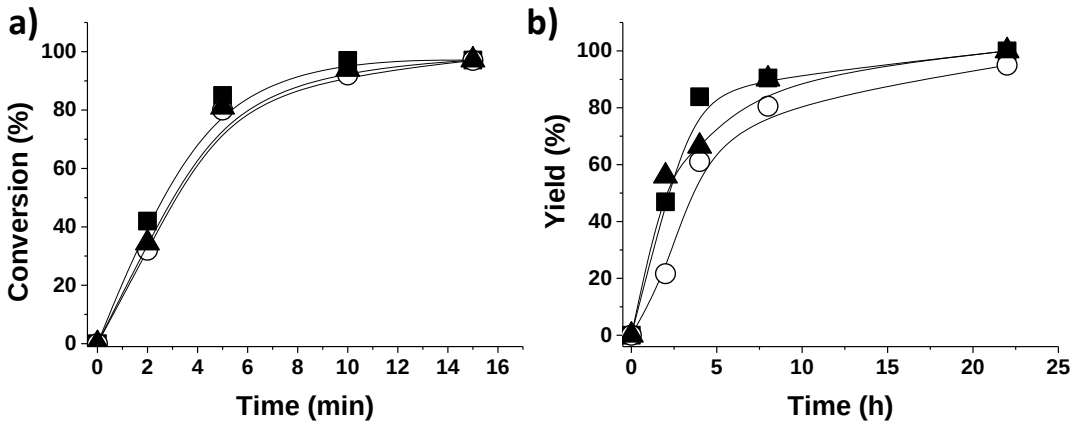

Figure 5. 5-hydroxymethylfurfural (HMF) oxidation (a) and 2,5-furandicarboxylic acid (FDCA) formation (b) using Pd/FLG (■), Pd/CNT (○) and Pd/CNF (▲) as catalyst Reaction conditions: Catalyst (10 mg), HMF (9.5 g L^{-1}; 75 mM), K_2CO_3 (21 g L^{-1}; 152 mM), 2 mL H_2O, 5 bar O_2, 160 °C.

From the temporal evolution of HMF conversion and FDCA formation it can be deduced that Pd/FLG is again more active than Pd/CNF, Pd/CNT being the less active material in the series. Heterogeneity of the process in the case of Pd/FLG was confirmed by performing a hot filtration test at 30% conversion and by analysis of the Pd in liquid phase at final reaction time. The results presented in supplementary information (Figure S11d and e) shows that although formation of FDCA does not progress upon removal of the solid catalyst, oxidation of HMF does not stop completely. This further progress of HMF oxidation could be attributed to the small percentage of Pd leached to the liquid phase (about 2 % of

the total initial Pd content in the Pd/FLG sample). Thus, both measurements hot filtration test and Pd analysis suggest the occurrence of a minor contribution to the catalysis of a homogeneous component due to the presence of leached Pd.

Stability of the catalyst was also studied by performing a series of consecutive reuses under the same reaction conditions (Figures S12-S15). As in the case of the hydrodeoxygenation of vanillin (V), also Pd/FLG undergoes a significant decay in the catalytic activity in the reuse, Pd/CNF being again the most stable material. Pd/CNT exhibits an intermediate performance between those of Pd/FLG and Pd/CNF. Reusability tests for Pd/CNF are presented in Figure 6, while supporting information contains information for the other two catalysts (Figures S12-S15).

In order to understand the origin of deactivation, TEM images of fresh and used supported Pd catalyst were compared. The particle size distributions for Pd NPs on the three carbon supports after use in 5-hydroxymethylfurfural oxidation are shown in Figures S16-S18, while Table 5 shows the distributions for all supported Pd catalysts. It was observed that in the case of Pd/FLG a remarkable increase in the Pd NP particle size from 2.6 ± 1.6 to 15.9 ± 11.3 occurs after the 5-hydroxymethylfurfural oxidation reaction. In the case of Pd/CNT observation of the presence of some scattered big Pd NP in the used sample is also observed. Considering that carboxylic acids are formed in the oxidation process and that by Coulombic interactions these compounds can increase the size of metal NPs, the data obtained by TEM images for Pd/FLG and Pd/CNT indicating a certain growth of Pd NPs are not without precedent. In the case of Pd/CNF the increase in Pd particle size is also clear, although it seems that the average is still sufficiently low (6.7 nm) to exhibit a good catalytic performance. Not surprisingly considering the mobilizing effect of carboxylic acids for metal

ions, palladium leaching from the solid catalyst to the solution was significantly higher for the oxidation of HMF than for the hydrodeoxygenation of vanillin (see Table 5), reaching in the worst case a Pd leaching of 6.6 % of the initial Pd content of the Pd/FLG.

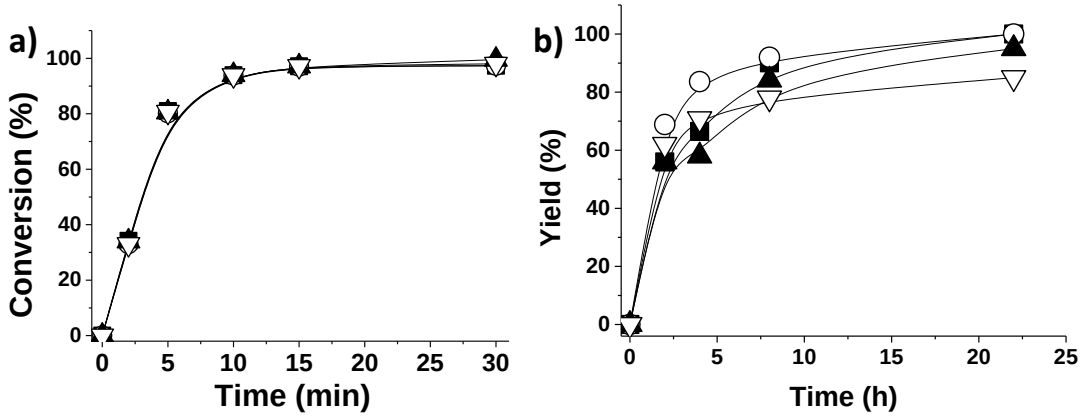

Figure 6. 5-hydroxymethylfurfural (HMF) conversion (a) and 2,5-furandicarboxylic acid (FDCA) formation (b) upon three consecutive uses of Pd/CNF as catalyst. Legend: First use (■), second use (○), third use (▲) and forth use (▽). Reaction conditions: Catalyst (10 mg), HMF (9.5 g L^{-1}; 75 mM), K_2CO_3 (21 g L^{-1}; 152 mM), 2 mL H_2O, 5 bar O_2, 160 °C.

Table 5. Palladium particle size distribution of the four-times used catalyst for vanillin hydrodeoxygenation or 5-hydroxymethylfurfural oxidation, palladium leaching and estimated TON and TOF for these reactions.

Entry	Catalyst	Reaction	Particle size (nm)	Pd Leaching (%)	TON	TOF (h^{-1})
1	Pd/CNT	Hydrodeoxygenation of V	3.4 ± 3.4	0.1	140	21
2	Pd/CNT	Oxidation of HMF	3.9 ± 3.6	3.0	80	813
3	Pd/FLG	Hydrodeoxygenation of V	2.3 ± 0.8	2.3	149	78
4	Pd/FLG	Oxidation of HMF	15.9 ± 11.3	6.6	85	829
5	Pd/CNF	Hydrodeoxygenation of V	2.8 ± 1.1	0.5	164	72
6	Pd/CNF	Oxidation of HMF	6.7 ± 11.3	2.1	94	901

TON : moles of converted substrate (V or HMF) divided moles of supported palladium after one use

TOF : moles of converted V or HMF divided moles of supported palladium at 1 and 0.083 h, respectively.

Conclusions

The present results have shown that although regardless the support Pd NPs exhibit a general catalytic activity for catalyzing hydrodeoxygenations and aerobic oxidations of interest in biomass transformation, the nature of the carbon support plays a significant role determining the activity of the fresh samples and the stability of Pd NPs under the reaction conditions. It has been found that Pd supported on FLG is initially the most active catalyst for both processes, but it undergoes deactivation in significant extent upon reuse. Among the causes of deactivation, poisoning in the case of hydrodeoxygenation and Pd particle size growth in the case of the aerobic oxidation appear the most probable ones. In this regard, CNFs as support presents a compromise between activity of the fresh material and stability

upon reuse. This role of CNFs has been interpreted as derived from the stabilization of particle size and the lack of poisoning by adsorption as indicated by elemental analysis. Characterization of the supported Pd catalyst has shown that for similar particle size and loading, it is not only the Pd dispersion the only parameter controlling the catalysis, but the nature and proportion of the basal, non-basal and defects planes of the support can have also a decisive importance in determining the activity and stability of the Pd NPs. In this regard, it seems that CNF exhibit a good balance with amorphous regions on the surface and basal and non-basal planes to stabilize Pd NPs.

Acknowledgements

Financial support by the Spanish Ministry of Economy and Competitiveness (Severo Ochoa GTQ2015-65163-C02-R1 and CTQ2014-53292-R) is gratefully acknowledged. Generalidad Valenciana is also thanked for funding (Prometeo 2017/063). S.N. thanks financial support by the Fundación Ramón Areces (XVIII Concurso Nacional para la Adjudicación de Ayudas a la Investigación en Ciencias de la Vida y de la Materia, 2016). C.R.C. thanks CONICYT for the financial support (Becas de doctorado en el extranjero "Becas Chile" - n° 72170200). The authors thank Dr. Tobias Placke (Universität Münster, Germany) for nitrogen adsorption measurements and adsorptive potential distributions calculations.

References

1. Corma, A.; Iborra, S.; Velty, A., Chemical routes for the transformation of biomass into chemicals. *Chem. Rev.* **2007,** 107, 2411-2502.
2. Huber, G. W.; Iborra, S.; Corma, A., Synthesis of transportation fuels from biomass: Chemistry, catalysts, and engineering. *Chem. Rev.* **2006,** 106, 4044-4098.
3. Navarro, R. M.; Peña, M. A.; Fierro, J. L. G., Hydrogen production reactions from carbon feedstocks: Fossil fuels and biomass. *Chem. Rev.* **2007,** 107, 3952-3991.
4. Zakzeski, J.; Bruijnincx, P. C. A.; Jongerius, A. L.; Weckhuysen, B. M., The catalytic valorization of lignin for the production of renewable chemicals. *Chem. Rev.* **2010,** 110, 3552-3599.
5. Chheda, J. N.; Huber, G. W.; Dumesic, J. A., Liquid-phase catalytic processing of biomass-derived oxygenated hydrocarbons to fuels and chemicals. *Angew. Chem. Int. Ed.* **2007,** 46, 7164-7183.
6. Zhou, C.-H.; Xia, X.; Lin, C.-X.; Tong, D.-S.; Beltramini, J., Catalytic conversion of lignocellulosic biomass to fine chemicals and fuels. *Chem. Soc. Rev* **2011,** 40, 5588-5617.
7. Crossley, S.; Faria, J.; Shen, M.; Resasco, D. E., Solid nanoparticles that catalyze biofuel upgrade reactions at the water/oil interface. *Science* **2010,** 327, 68-72.
8. Xu, X.; Li, Y.; Gong, Y.; Zhang, P.; Li, H.; Wang, Y., Synthesis of palladium nanoparticles supported on mesoporous n-doped carbon and their catalytic ability for biofuel upgrade. *J. Am. Chem. Soc* **2012**, 16987-16990.
9. Lam, E.; Luong, J. H., Carbon Materials as Catalyst Supports and Catalysts in the Transformation of Biomass to Fuels and Chemicals. *ACS Catal.* **2014,** 4, 3393−3410.
10. Navalon, S.; Dhakshinamoorthy, A.; Alvaro, M.; Garcia, H., Metal nanoparticles supported on two-dimensional graphenes as heterogeneous catalysts. *Coord. Chem. Rev.* **2016,** 312, 99-148.
11. Wildgoose, G. G.; Banks, C. E.; Compton, R. G., Metal nanoparticles and related materials supported on Carbon nanotubes: Methods and applications. *Small* **2006,** 2, 182-193.
12. Zhu, J.; Holmen, A.; Chen, D., Carbon nanomaterials in catalysis: proton affinity, chemical and electronic properties, and their catalytic consequences. *ChemCatChem* **2013,** 5, 378-401.
13. Xia, H.; An, J.; Hong, M.; Xu, S.; Zhang, L.; Zuo, S., Aerobic oxidation of 5-hydroxymethylfurfural to 2,5-difurancarboxylic acid over Pd-Au nanoparticles supported on Mg-Al hydrotalcite. *Catal. Today* **2019,** 319, 113-120.
14. Calvo-Flores, F. G.; Dobado, J. A., Lignin as renewable raw material. *ChemSusChem* **2010,** 3, 1227-1235
15. Upton, B. M.; Kasko, A. M., Strategies for the conversion of lignin to high-value polymeric materials: Review and perspective. *Chem. Rev.* **2016,** 116, 2275-2306.
16. Zhang, F.; Jin, Y.; Fu, Y.; Zhong, Y.; Zhu, W.; Ibrahim, A. A.; El-Shall, M. S., Palladium nanoparticles incorporated within sulfonic acid-functionalized MIL-101(Cr) for efficient catalytic conversion of vanillin. *J. Mater. Chem. A* **2015,** 3, 17008-17015.
17. Santos, J. L.; Alda-Onggar, M.; Fedorov, V.; Peurla, M.; Eranen, K.; Maki-Arvela, P.; Centeno, M. A.; Murzin, D. Y., Hydrodeoxygenation of vanillin over carbon supported metal catalysts. *Appl. Catal. A.-Gen.* **2018,** 561, 137-149.
18. Hao, P.; Schwartz, D. K.; Medlin, J. W., Phosphonic acid promotion of supported Pd catalysts for low temperature vanillin hydrodeoxygenation in ethanol. *Appl. Catal. A.-Gen.* **2018,** 561, 1-6.
19. Zhang, F.; Zheng, S.; Xiao, Q.; Zhong, Y.; Zhu, W.; Lin, A.; Samy El-Shall, M., Synergetic catalysis of palladium nanoparticles encaged within amine-functionalized UiO-66 in the hydrodeoxygenation of vanillin in water. *Green Chem.* **2016,** 18, (9), 2900-2908.

20. Davis, S. E.; Ide, M. S.; Davis, R. J., Selective oxidation of alcohols and aldehydes over supported metal nanoparticles. *Green Chem.* **2013,** 15, 17-45.
21. Dutta, S.; De, S.; Saha, B., A brief summary of the synthesis of polyester building-block chemicals and biofuels from 5-hydroxymethylfurfural *ChemPlusChem* **2012,** 77, 259-272.
22. Zhang, Z.; Deng, K., Recent advances in the catalytic synthesis of 2,5-furandicarboxylic acid and its derivatives. *ACS Catal.* **2015,** 5, 6529-6544.
23. Teong, S. P.; Yi, G.; Zhang, Y., Hydroxymethylfurfural production from bioresources: Past, present and future. *Green Chem.* **2014,** 16, 2015-2026.
24. Siyo, B.; Schneider, M.; Radnik, J.; Pohl, M.-M.; Langer, P.; Steinfeldt, N., Influence of support on the aerobic oxidation of HMF into FDCA over preformed Pd nanoparticle based materials. *Appl. Catal. A.-Gen.* **2014,** 478, 107-116.
25. Davis, S. E.; Houk, L. R.; Tamargo, E. C.; Datye, A. K.; Davis, R. J., Oxidation of 5-hydroxymethylfurfural over supported Pt, Pd and Au catalysts. *Catal. Today* **2011,** 160, (1), 55-60.
26. Rathod, P. V.; Jadhav, V. H., Efficient Method for Synthesis of 2,5-Furandicarboxylic Acid from 5-Hydroxymethylfurfural and Fructose Using Pd/CC Catalyst under Aqueous Conditions. *ACS Sustain. Chem. Eng.* **2018,** 6, (5), 5766-5771.
27. Toebes, M. L.; van Dillen, J. A.; de Jong, K. P., Synthesis of supported palladium catalysts. *J. Mol. Catal. A.-Chem.* **2001,** 173, 75-98.
28. Suh, D. J.; Park, T.-J.; Ihm, S.-K., Effect of surface oxygen groups of carbon supports on the characteristics of Pd/C catalysts. *Carbon* **1993,** 31, 427-435.
29. Kang, M.; Song, M. W.; Kim, K. L., Palladium catalysts supported on activated carbon with different textural and surface chemical properties. *React. Kinet. Catal. L.* **2002**, 207-212.
30. Placke, T.; Siozios, V.; Rothermel, S.; Meister, P.; Colle, C.; Winter, M., Assessment of Surface Heterogeneity: a Route to Correlate and Quantify the 1st Cycle Irreversible Capacity Caused by SEI Formation to the Various Surfaces of Graphite Anodes for Lithium Ion Cells. *Z. Phys. Chem.* **2015**, 1451.
31. Machado, B. F.; Oubenali, M.; Axet, M. R.; NGuyen, T. T.; Tunckol, M.; Girleanu, M.; Ersen, O.; Gerber, I. C.; Serp, P., Understanding the surface chemistry of carbon nanotubes: Toward a rational design of Ru nanocatalysts. *J. Catal.* **2014,** 309, 185-198.
32. Placke, T.; Siozios, V.; Schmitz, R.; Lux, S. F.; Bieker, P.; Colle, C.; Meyer, H.-W.; Passerini, S.; Winter, M., Influence of graphite surface modifications on the ratio of basal plane to "non-basal plane" surface area and on the anode performance in lithium ion batteries. *J. Power Sources* **2012,** 200, 83-91.
33. Reshetenko, T. V.; Avdeeva, L. B.; Ismagilov, Z. R.; Pushkarev V.V.; Cherepanov, S. V.; Chuvilin, A. L.; Likholobov, V. A., Catalytic filamentous carbon: Structural and textural properties. *Carbon* **2003,** 41, 1605-1615.
34. Estrade-Szwarckopf, H., XPS photoemission in carbonaceous materials: A ''defect'' peak beside the graphitic asymmetric peak. *Carbon* **2004,** 42, 1713-1721.
35. Ganesan, K.; Ghosh, S.; Krishna, N. G.; Ilango, S.; Kamruddin, M.; Tyagi, A. K., A comparative study on defect estimation using XPS and Raman spectroscopy in few layer nanographitic structures. *Phys. Chem. Chem. Phys.* **2016,** 18, 22160-22167
36. Okpalugo, T. I. T.; Papakonstantinou, P.; Murphy, H.; McLaughlin, J.; Brown, N. M. D., High resolution XPS characterization of chemical functionalised MWCNTs and SWCNTs. *Carbon* **2005,** 43, 153-161.
37. Müller, J.-O.; Su, D. S.; Wild, U.; Schlögl, R., Bulk and surface structural investigations of diesel engine soot and carbon black. *Phys. Chem. Chem. Phys.* **2007,** 9, 4018-4025.

38. Cançado, L. G.; Jorio, A.; Martins Ferreira, E. H.; Stavale, F.; Achete, C. A.; Capaz, R. B.; Moutinho, M. V. O.; Lombardo, A.; Kulmala, T. S.; Ferrari, A. C., Quantifying Defects in Graphene via Raman Spectroscopy at Different Excitation Energies. *Nano Lett.* **2011,** 11, 3190-3196.
39. Cançado, L. G.; Takai, K.; Enoki, T., General equation for the determination of the crystallite size La of nanographite by Raman spectroscopy. *Appl. Phys. Lett.* **2006,** 88, 163106.
40. Domínguez-Domínguez, S.; Berenguer-Murcia, A.; Pradhan, B. K.; Linares-Solano, A.; Cazorla-Amorós, D., Semihydrogenation of Phenylacetylene Catalyzed by Palladium Nanoparticles Supported on Carbon Materials. *J. Phys. Chem. C,* **2008,** 112, 3827-3834.

Supporting Information

Influence of carbon supports on palladium nanoparticles activity for hydrodeoxygenation and aerobic oxidation in biomass transformations

Juan C. Espinosa,[a] Ruben Castro Contreras,[b] Sergio Navalón,[a] Camila Rivera-Cárcamo,[b] Mercedes Álvaro,[a] Bruno F. Machado,[c] Philippe Serp,[b]* Hermenegildo Garcia[*,a,d]

[a] Departamento de Química and Instituto de Tecnología Química CSIC-UPV, Universidad Politécnica de Valencia, Consejo Superior de Investigaciones Científicas, Av. de los Naranjos s/n, 46022 Valencia, Spain

[b]*LCC-CNRS, Université de Toulouse, CNRS, INPT, Toulouse, France*

[c]*Laboratory of Separation and Reaction Engineering - Laboratory of Catalysis and Materials (LSRE-LCM), Chemical Engineering Department, Faculty of Engineering, University of Porto, Rua Dr. Roberto Frias s/n, 4200-465 Porto, Portugal*

[d] Center of Excellence for Advanced Materials Research, King Abdulaziz University, Jeddah, Saudi Arabia

[¥] Both are first authors

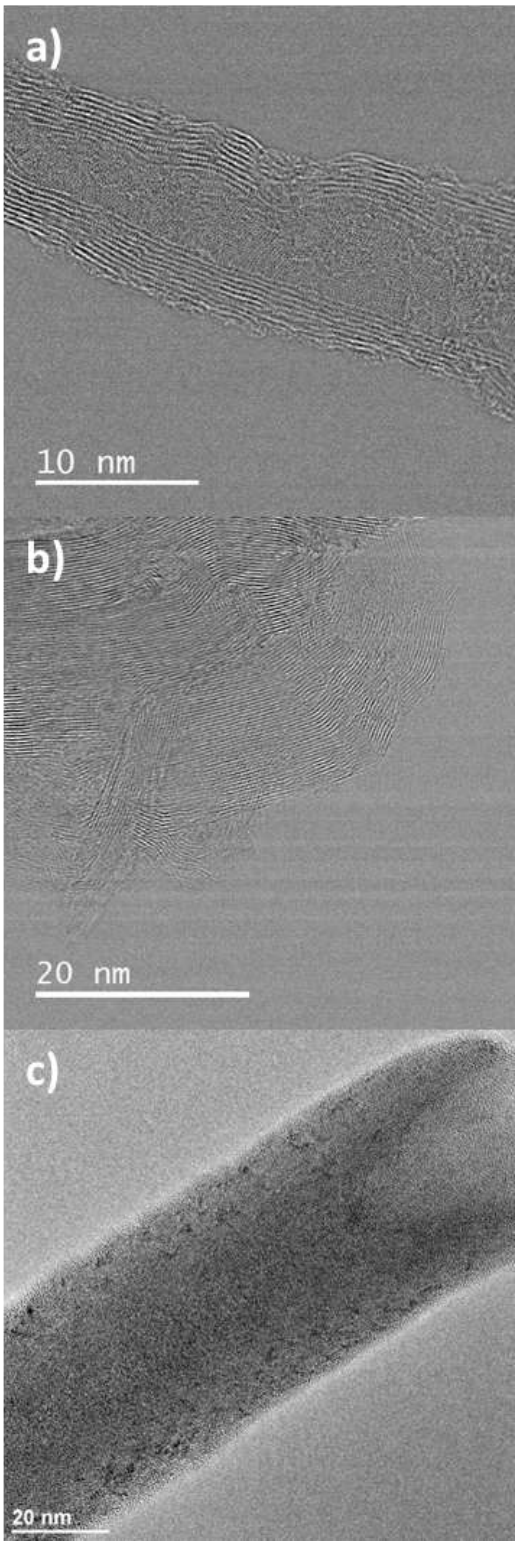

Figure S1. TEM micrographs of: a) CNT_{COOH}; b) FLG_{COOH}; and c) CNF_{COOH} supports.

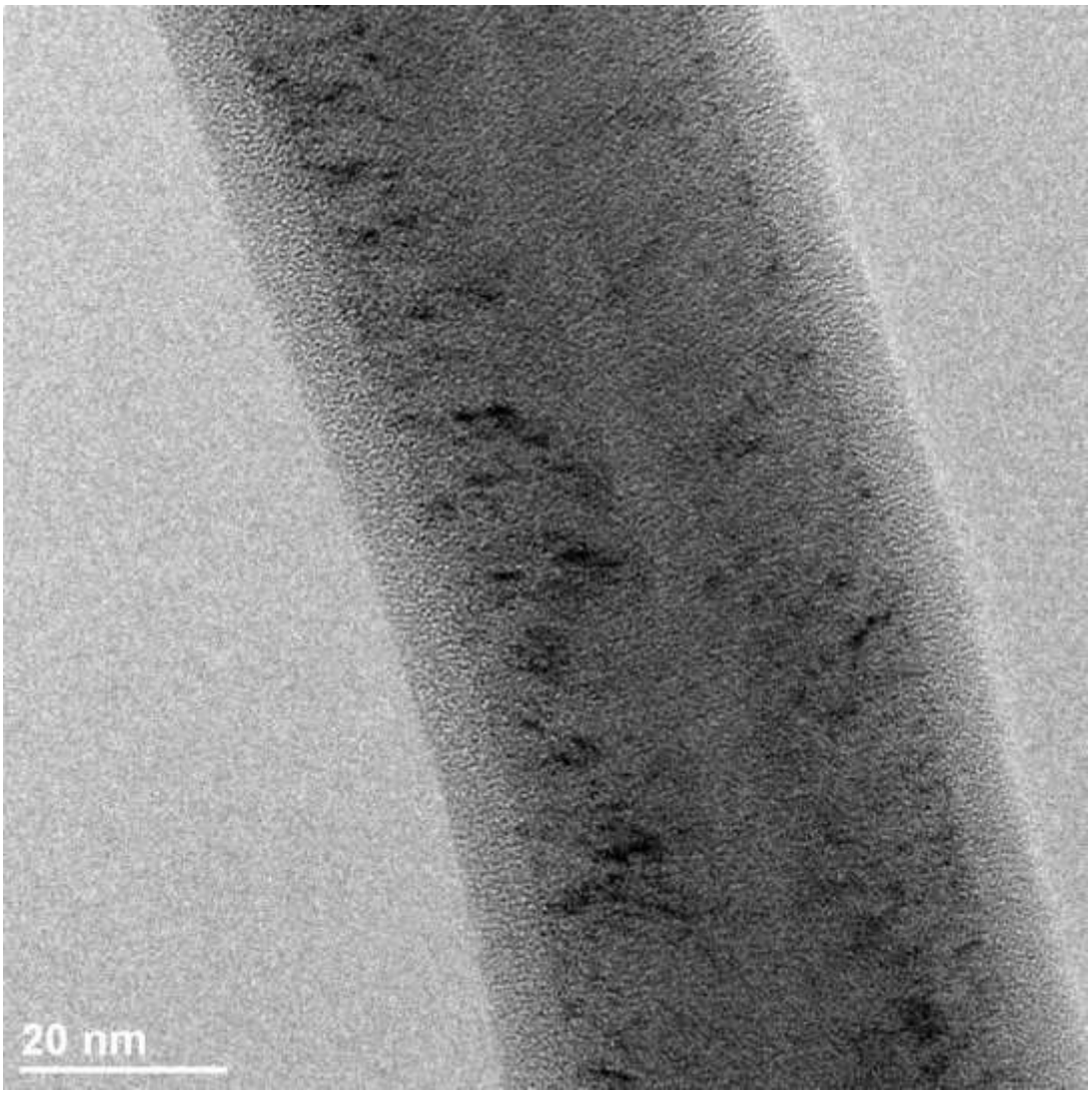

Figure S2. TEM micrographs of CNF_{COOH} support showing the presence of disordered carbon on the surface.

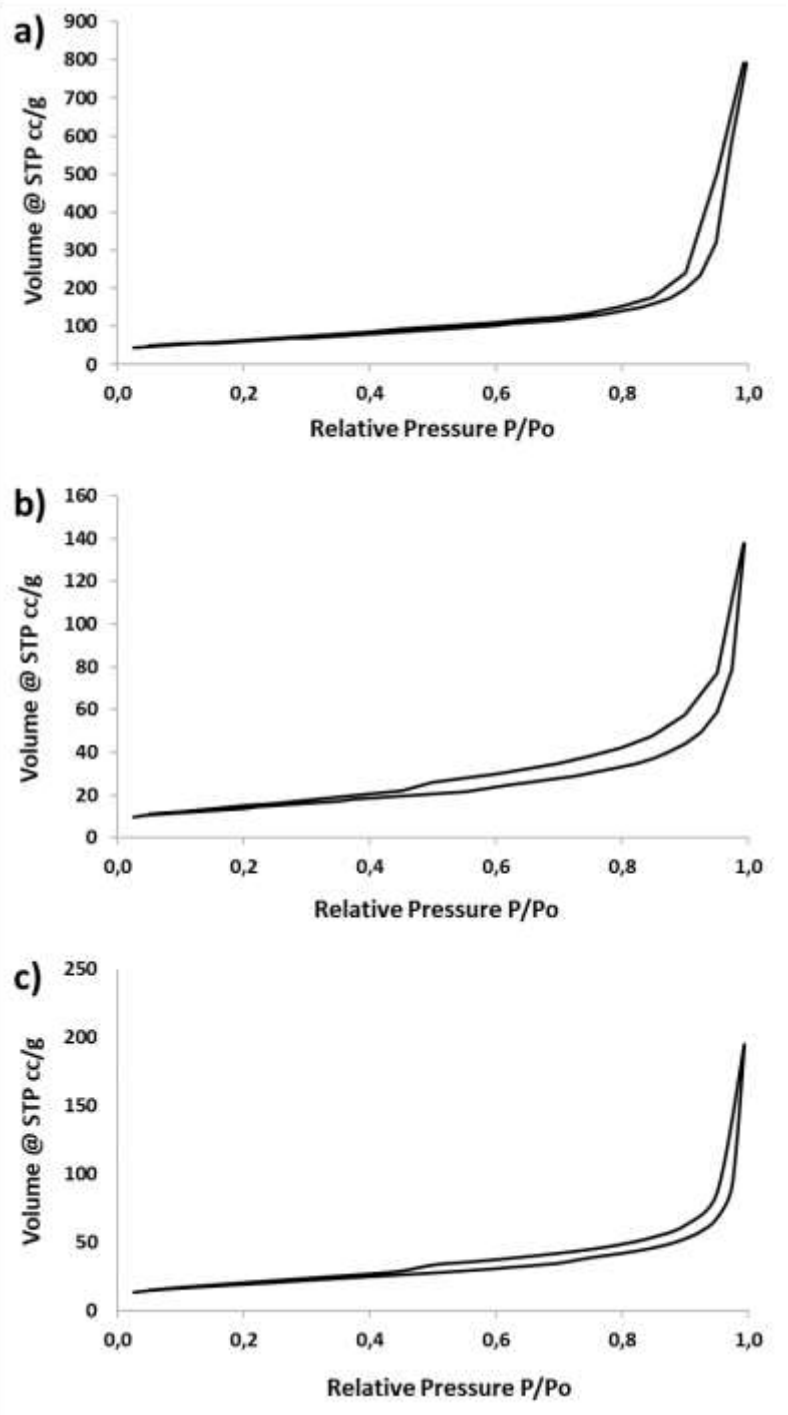

Figure S3. Nitrogen isotherms of: a) CNT_{COOH}; b) FLG_{COOH}; and c) CNF_{COOH} supports.

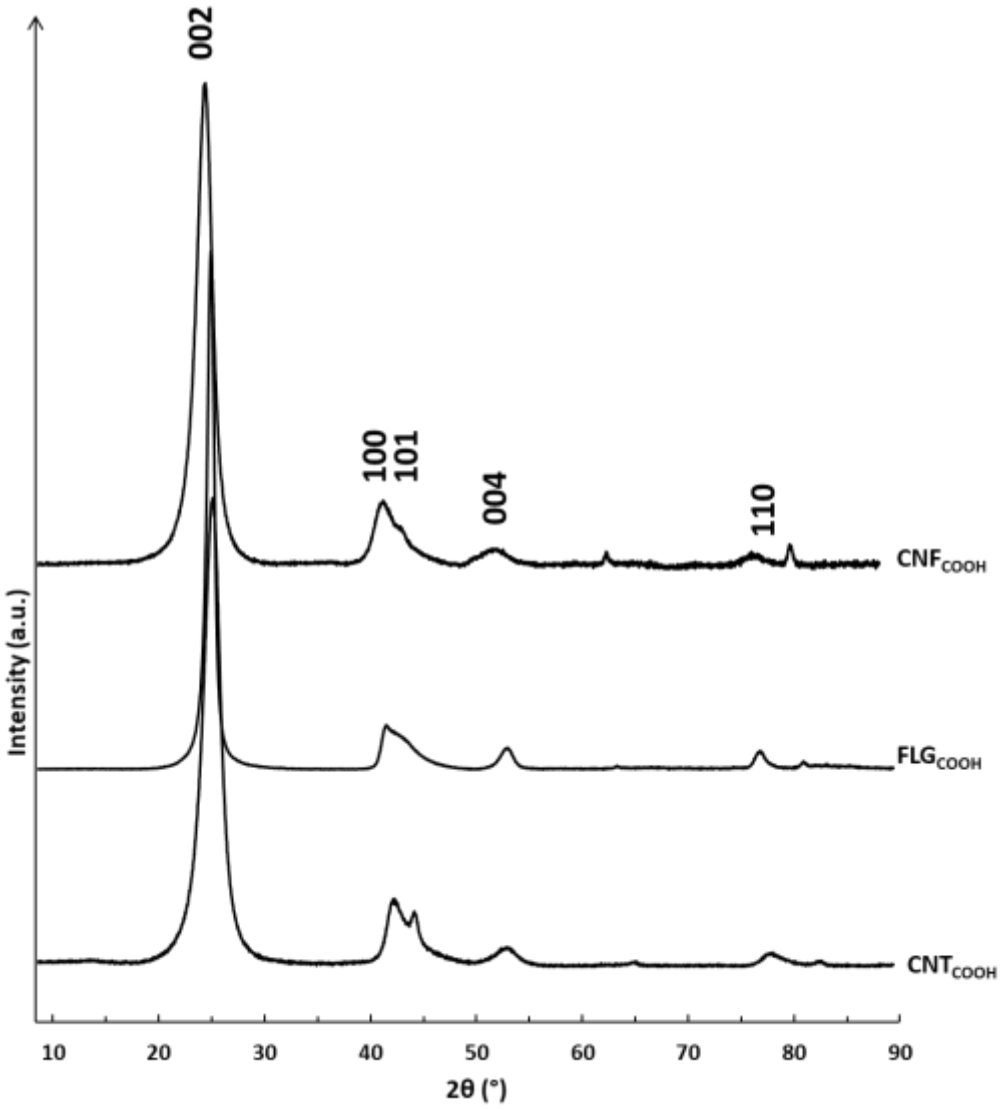

Figure S4. XRD patterns of CNT_{COOH}, FLG_{COOH} and CNF_{COOH} supports.

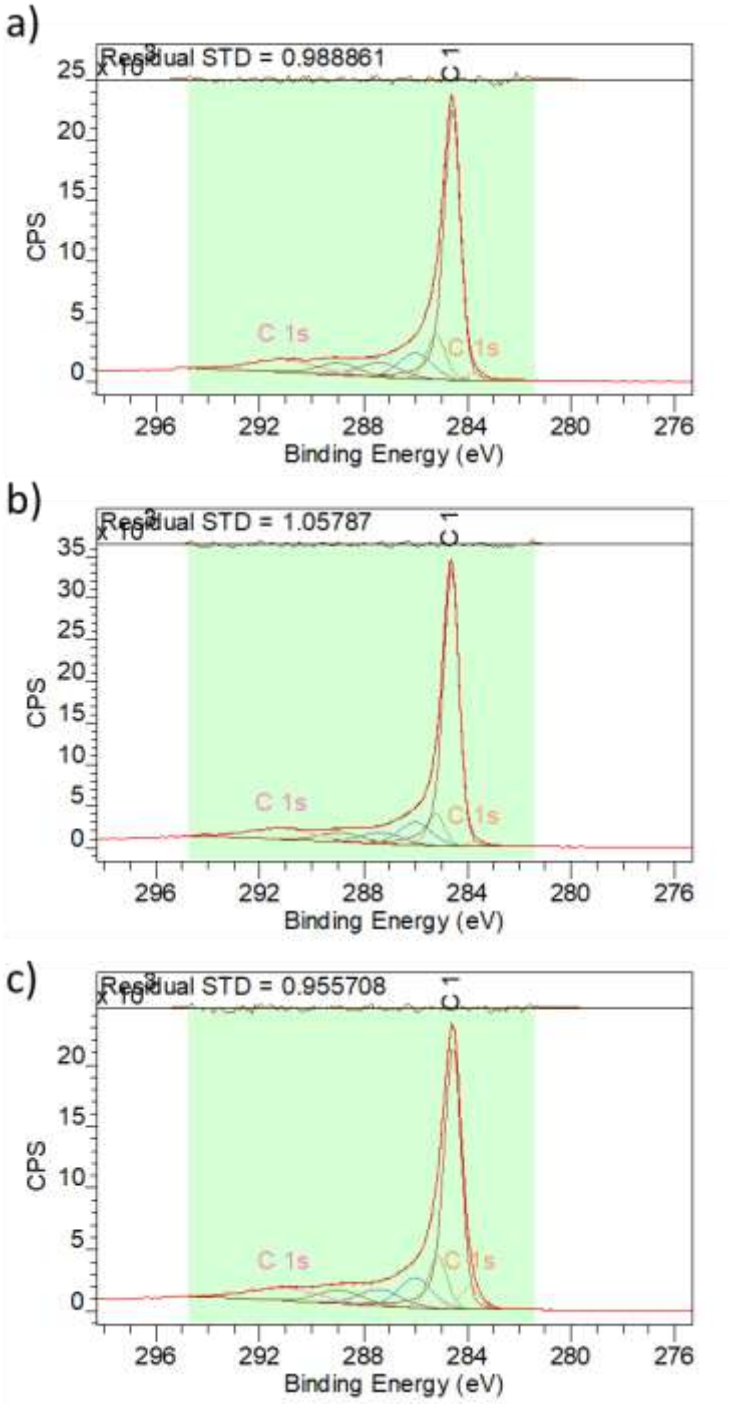

Figure S5. XP spectra of C 1s for: a) CNT_{COOH}; b) FLG_{COOH}; and c) CNF_{COOH} supports.

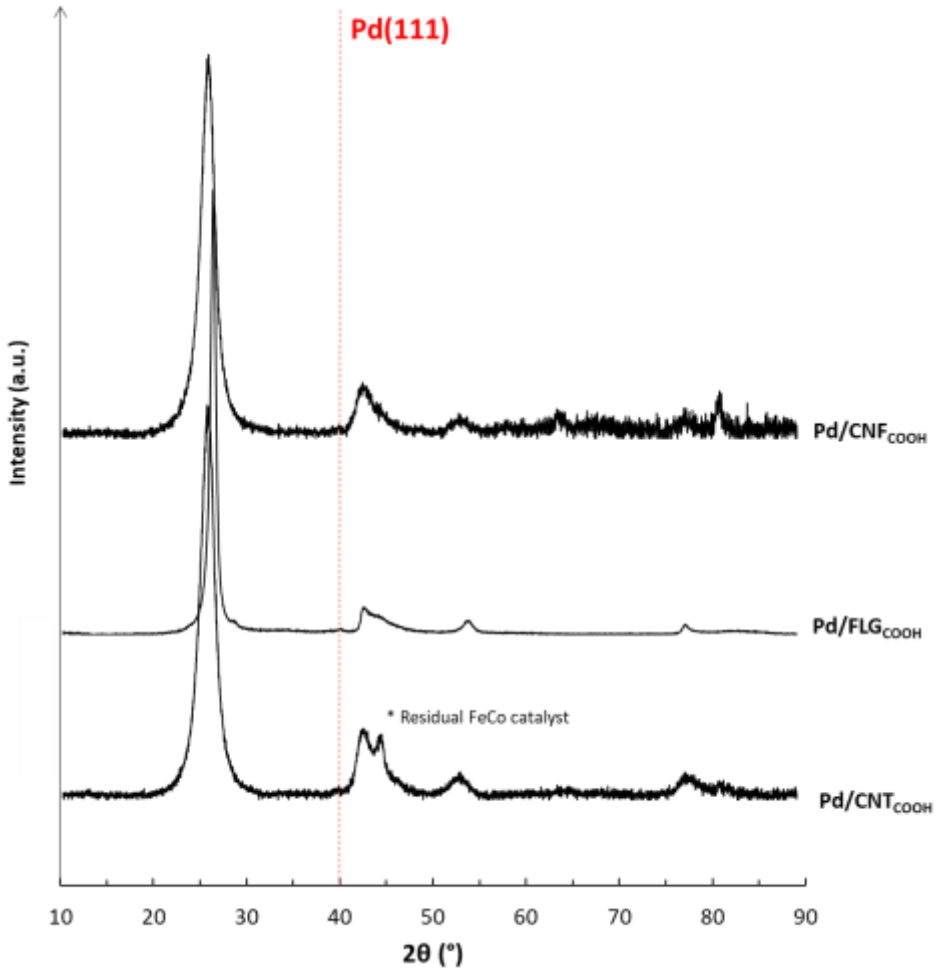

Figure S6. XRD patterns of Pd/CNT$_{COOH}$, Pd/FLG$_{COOH}$ and Pd/CNF$_{COOH}$ supports.

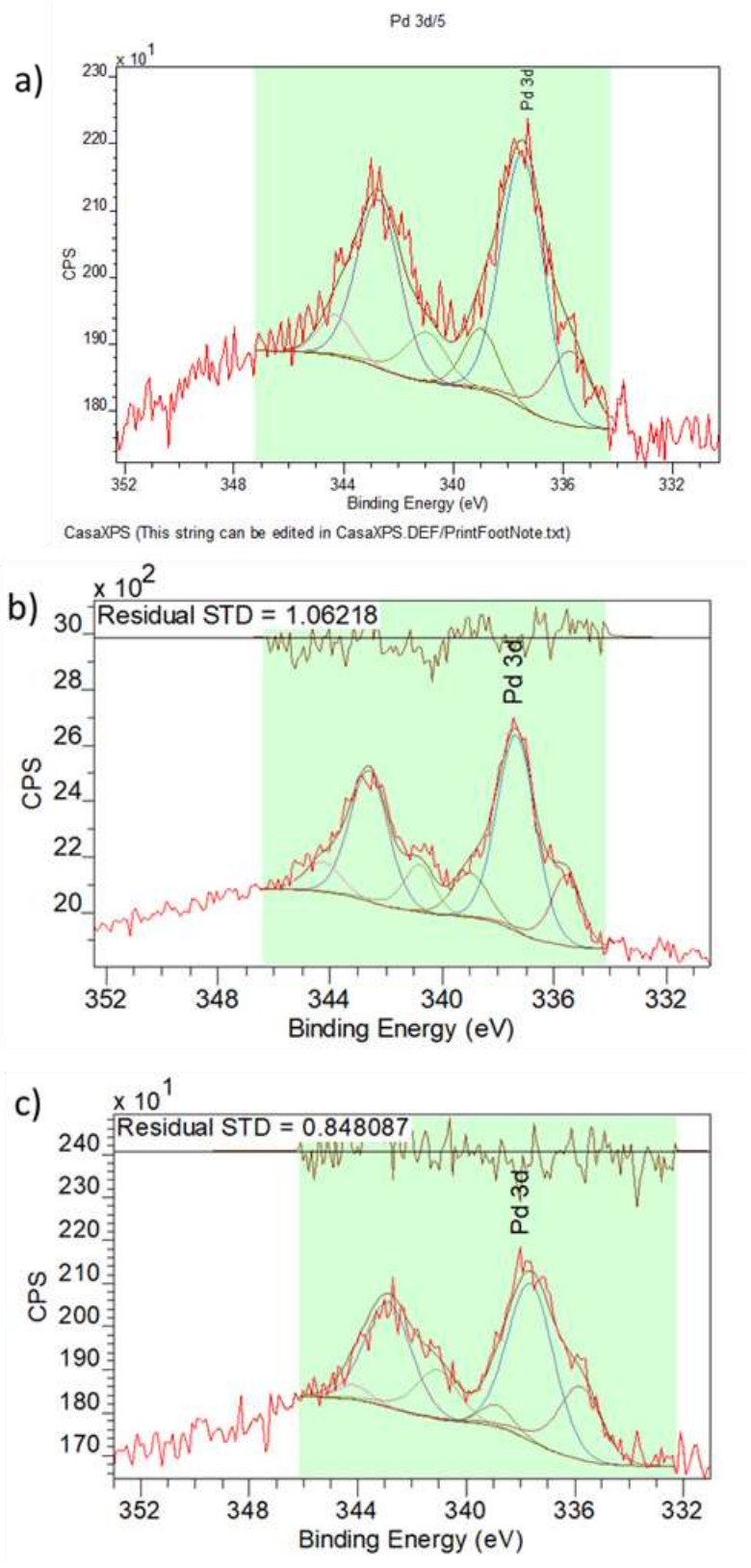
a)
Pd 3d/5
x 10^1
CPS
Pd 3d
Binding Energy (eV)
CasaXPS (This string can be edited in CasaXPS.DEF/PrintFootNote.txt)
b)
x 10^2
Residual STD = 1.06218
CPS
Pd 3d
Binding Energy (eV)
c)
x 10^1
Residual STD = 0.848087
CPS
Pd 3d
Binding Energy (eV)

Figure S7. XP spectra of Pd 3d for: a) Pd/CNT_{COOH}; b) Pd/FLG_{COOH}; and c) Pd/CNF_{COOH} catalysts.

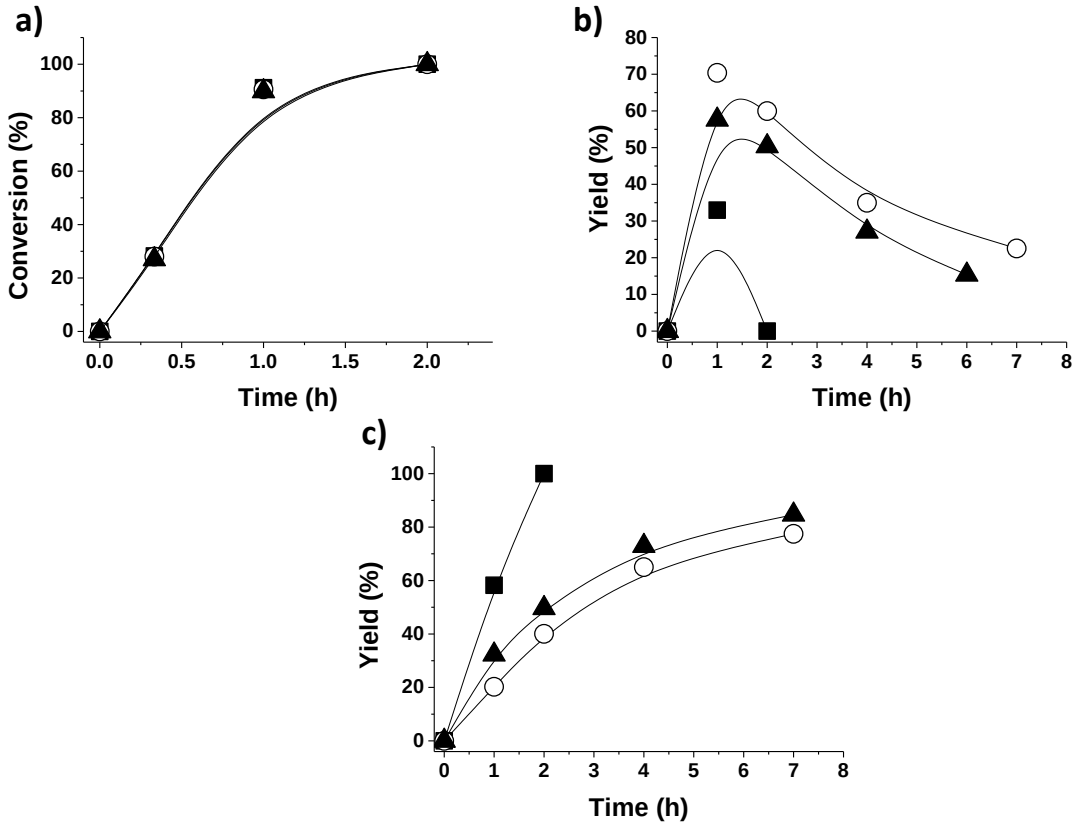

Figure S8. Vanillin (V) conversion (a), vanillyl alcohol (VA) evolution (b) and 2-methoxy-4-methylphenol (MMP) (c) formation using Pd/FLG as catalyst during three consecutive uses. Legend: First use (■), second use (○) and third use (▲). Reaction conditions: Catalyst (10 mg), vanillin (20 g L^{-1}; 0.13 M), 2 mL H_2O, 5 bar H_2, 100 °C.

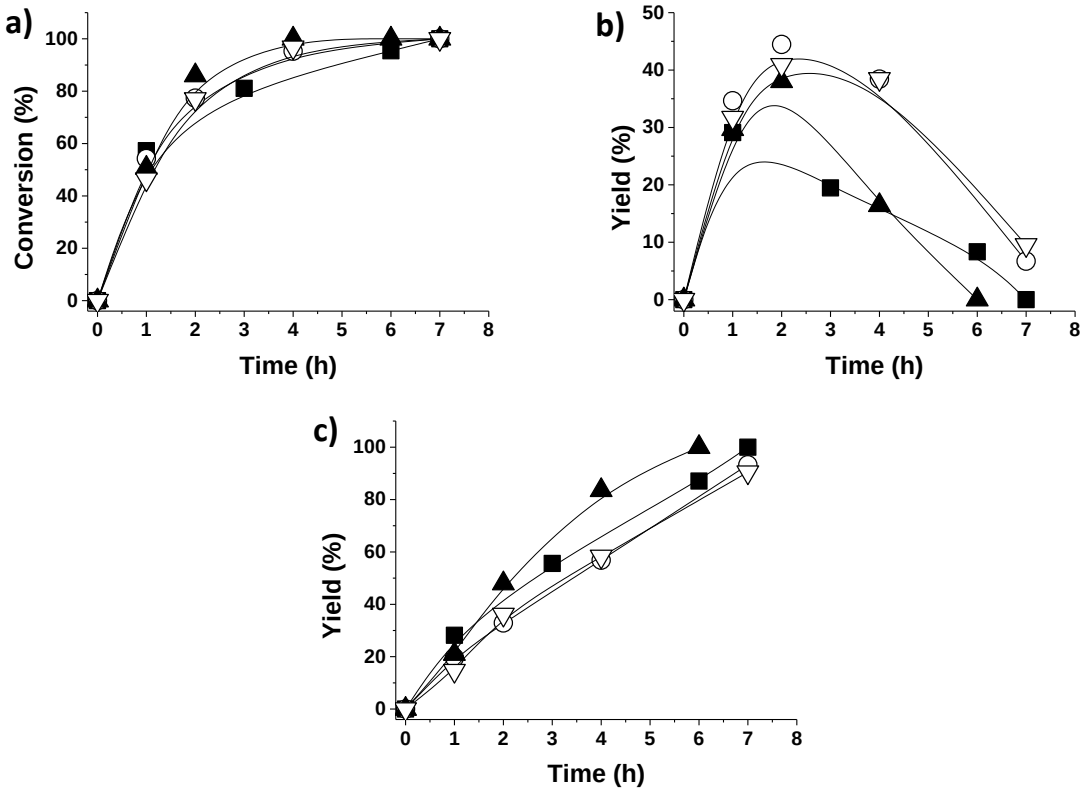

Figure S9. Vanillin (V) conversion (a), vanillyl alcohol (VA) evolution (b) and 2-methoxy-4-methylphenol (MMP) (c) formation using Pd/CNT as catalyst during four consecutive uses. Legend: First use (■), second use (○), third use (▲) and forth use (▽). Reaction conditions: Catalyst (10 mg), vanillin (20 g L^{-1}; 0.13 M), 2 mL H_2O, 5 bar H_2, 100 °C.

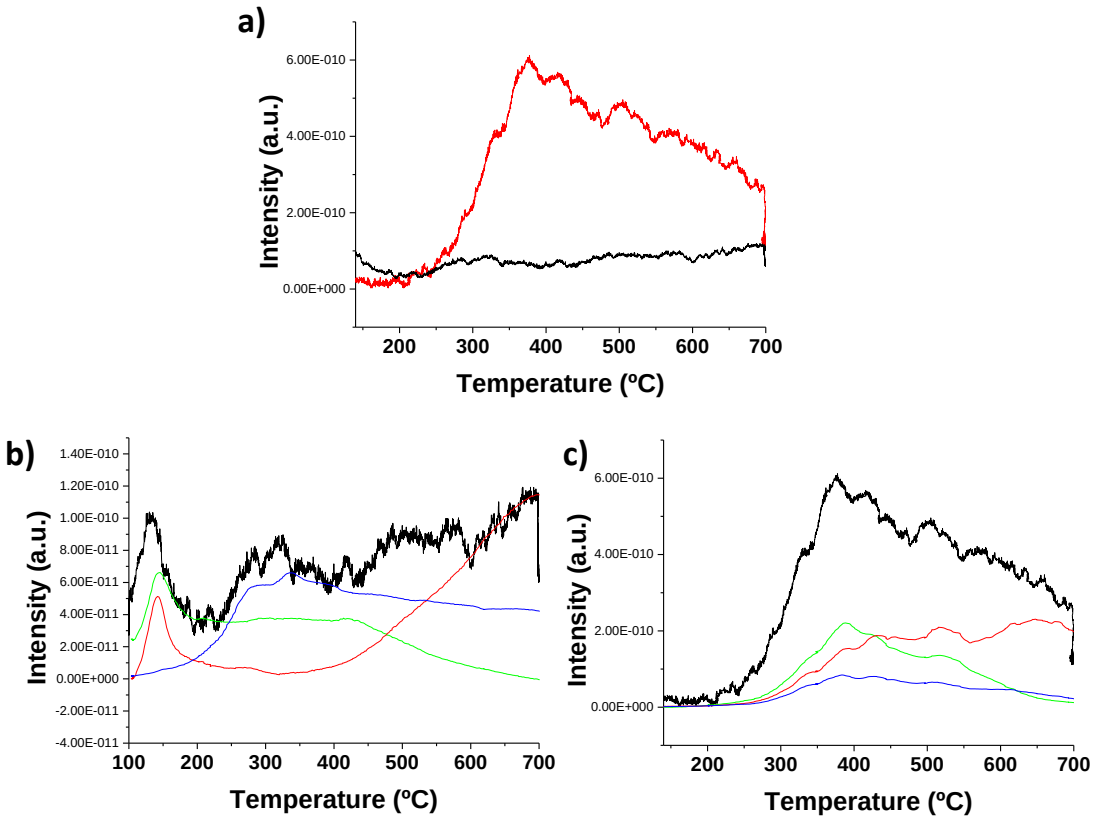

Figure S10. TPD profile (a) for fresh Pd/FLG (black line) and used Pd/FLG (red line) for vanillin hydrodeoxygenation reaction, and TPD-MS profile for fresh (b) and used (c) Pd/FLG catalyst. Legend: H_2O (green line), CO (red line), CO_2 (blue line).

Table S1. Elemental analysis for the three used catalysts, fresh and after use.	
Catalyst	**% C**
Pd/CNT[a]	88.4
Pd/CNF[a]	93.7
Pd/FLG[a]	95.1
Pd/CNT[b]	86.0
Pd/CNF[b]	91.8
Pd/FLG[b]	92.3
Pd/CNT[c]	89.2
Pd/CNF[c]	91.0
Pd/FLG[c]	86.7
a) Fresh catalyst; b) Catalyst after use; c) Catalyst after use in the reaction with additional 30% of MMP as poisoning agent.	

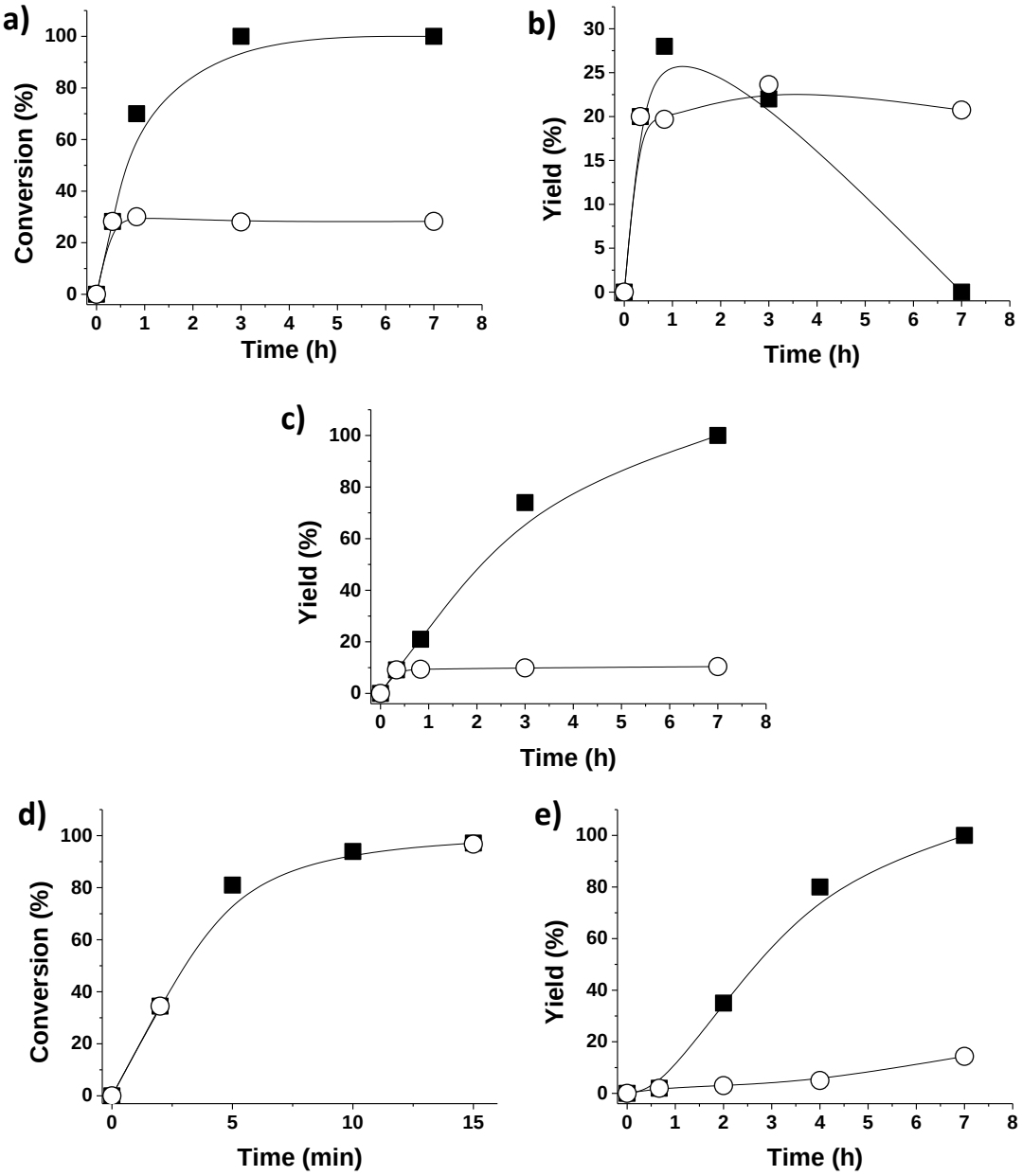

Figure S11. Hot filtration tests for vanillin hydrodeoxygenation (a, b, c) and 5-hydroxymethylfurfural oxidation (d, e) using Pd/CNF as catalyst. Legend: Vanillin (V) conversion (a), vanillyl alcohol (VA) evolution (b), 2-methoxy-4-methylphenol (MMP) formation (c), 5-hydroxymethylfurfural (HMF) conversion (d), 2,5-furandicarboxylic acid (FDCA) formation (e). Close (■) and open symbols (○) represent the reaction evolution in

the presence and in the absence of Pd/CNF, respectively. Reaction conditions for vanillin hydrodeoxygenation: Catalyst (10 mg), vanillin (20 g L^{-1}; 0.13 M), H_2O (2 mL), 5 bar H_2, 100 °C, filtration after 30 minutes reaction. Reaction conditions for 5-hydroxymethylfurfural oxidation: Catalyst (10 mg), HMF (9.5 g L^{-1}; 75 mM), K_2CO_3 (21 g L^{-1}; 152 mM), H_2O (2 mL), 5 bar O_2, 160 °C, filtration after 2 minutes reaction.

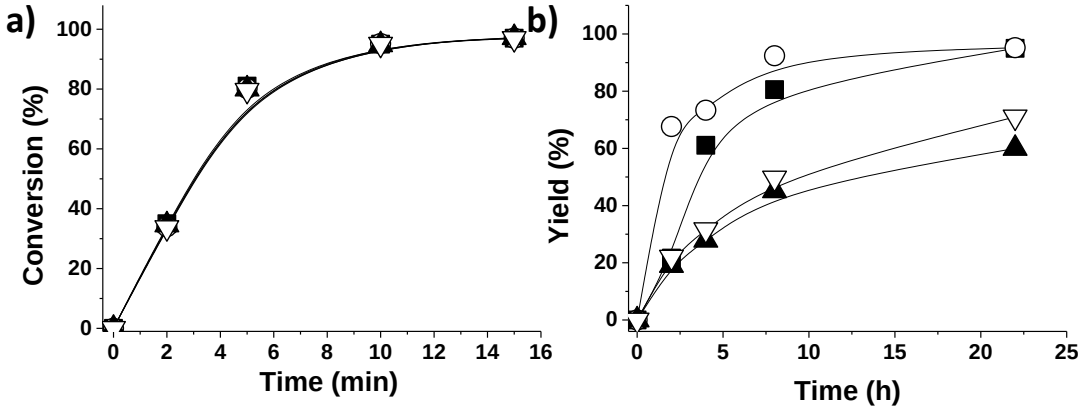

Figure S12. 5-hydroxymethylfurfural (HMF) conversion (a) and 2,5-furandicarboxylic acid (FDCA) formation (b) using Pd/CNT as catalyst. Legend: First use (■), second use (○), third use (▲) and forth use (▽). Reaction conditions: Catalyst (10 mg), HMF (9.5 g L^{-1}; 75 mM), K_2CO_3 (21 g L^{-1}; 152 mM), 2 mL H_2O, 5 bar O_2, 160 °C.

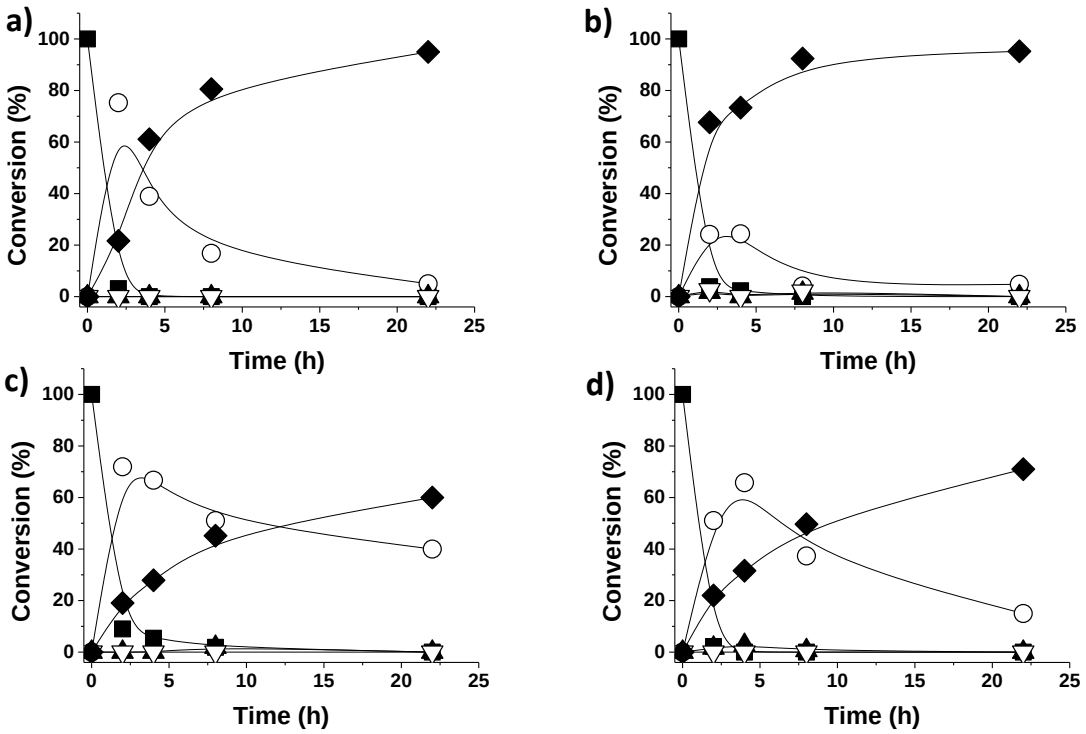

Figure S13. 5-hydroxymethylfurfural (HMF) oxidation, 2,5-furandicarboxylic acid (FDCA) and intermediates HMFCA, DFF and FFCA formation using Pd/CNT as catalyst during four consecutive uses. Legend: First use (a), second use (b), third use (c) and forth use (d). HMF (■), HMFCA (○), DFF (▲), FFCA (▽) and FDCA (◆). Reaction conditions: Catalyst (10 mg), HMF (9.5 g L^{-1}; 75 mM), K_2CO_3 (21 g L^{-1}; 152 mM), 2 mL H_2O, 5 bar O_2, 160 °C.

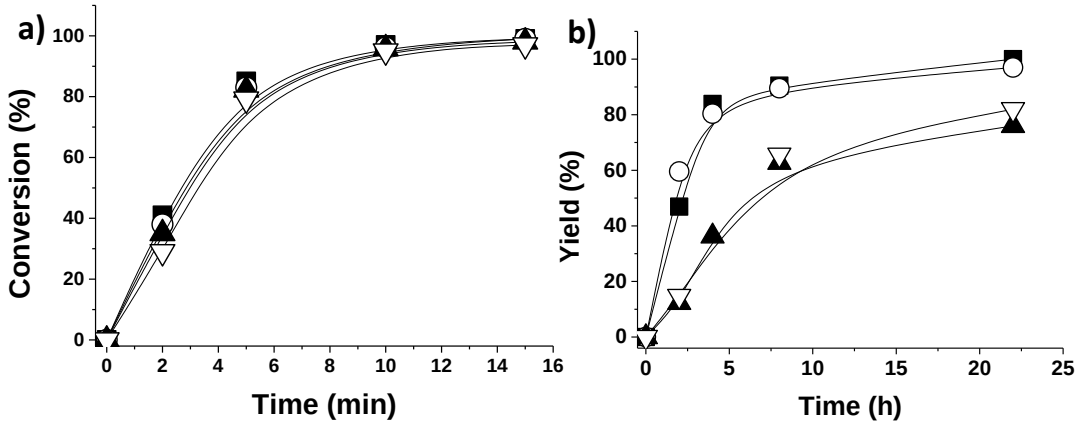

Figure S14. 5-hydroxymethylfurfural (HMF) conversion (a) and 2,5-furandicarboxylic acid (FDCA) formation (b) using Pd/FLG as catalyst. Legend: First use (■), second use (○), third use (▲) and forth use (▽). Reaction conditions: Catalyst (10 mg), HMF (9.5 g L^{-1}; 75 mM), K_2CO_3 (21 g L^{-1}; 152 mM), 2 mL H_2O, 5 bar O_2, 160 °C.

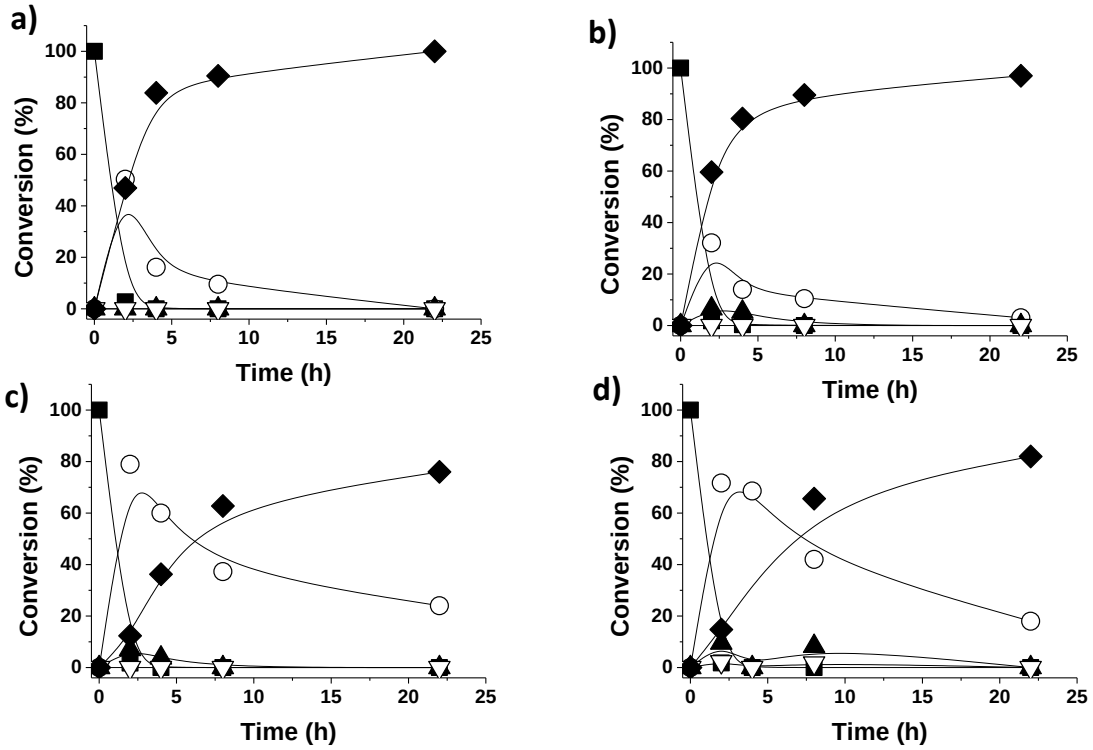

Figure S15. 5-hydroxymethylfurfural (HMF) oxidation, 2,5-furandicarboxylic acid (FDCA) and intermediates HMFCA, DFF and FFCA formation using Pd/FLG as catalyst during four consecutive uses. Legend: First use (a), second use (b), third use (c) and forth use (d). HMF (■), HMFCA (○), DFF (▲), FFCA (▽) and FDCA (◆). Reaction conditions: Catalyst (10 mg), HMF (9.5 g L^{-1}; 75 mM), K_2CO_3 (21 g L^{-1}; 152 mM), 2 mL H_2O, 5 bar O_2, 160 °C.

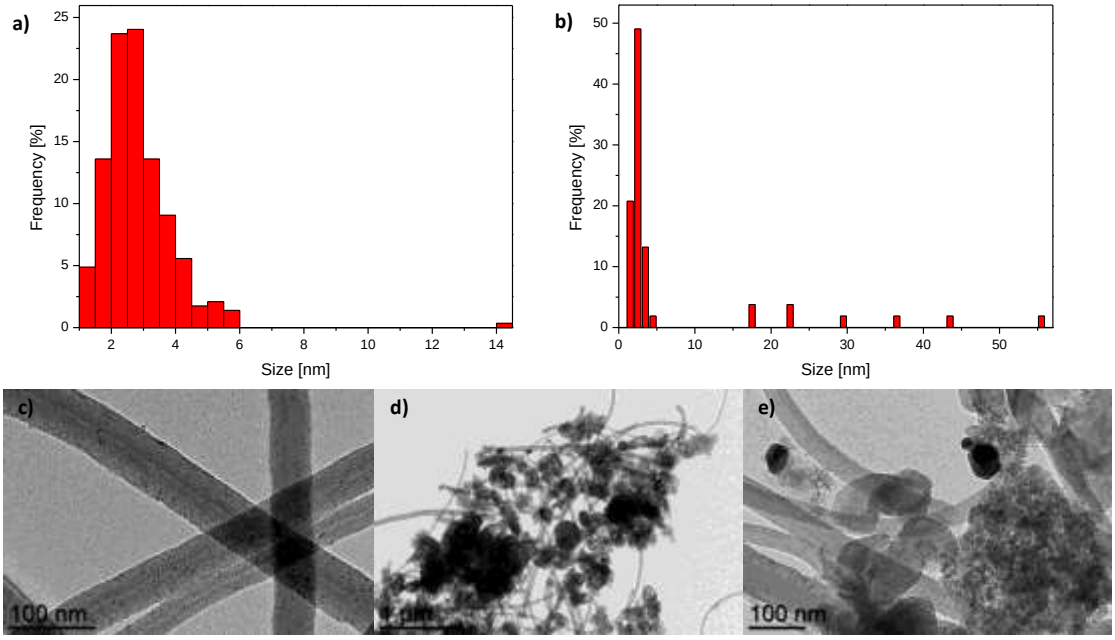

Figure S16. Pd particle size distribution (a, b) and TEM images (c, d, e) for Pd/CNF after four consecutive uses for the vanillin hydrodeoxygenation reaction (a, c) and 5-hydroxymethylfurfural oxidation (b, d, e).

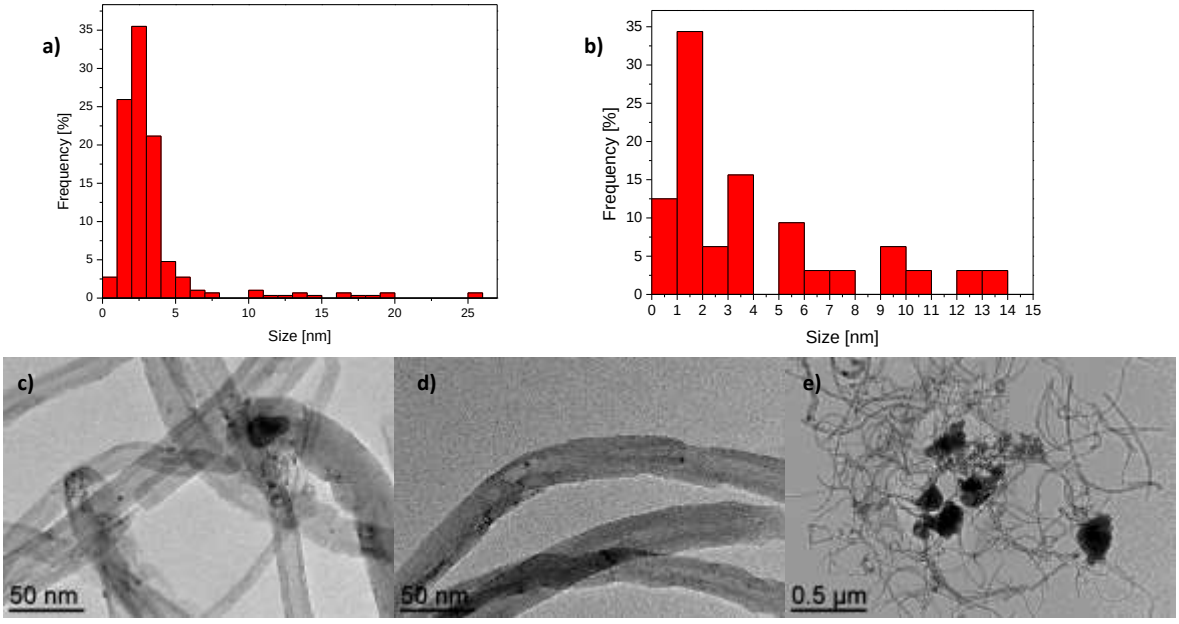

Figure S17. Pd particle size distribution (a, b) and TEM images (c, d, e) for Pd/CNT after four consecutive uses for the vanillin hydrodeoxygenation reaction (a, c) and 5-hydroxymethylfurfural oxidation (b, d, e).

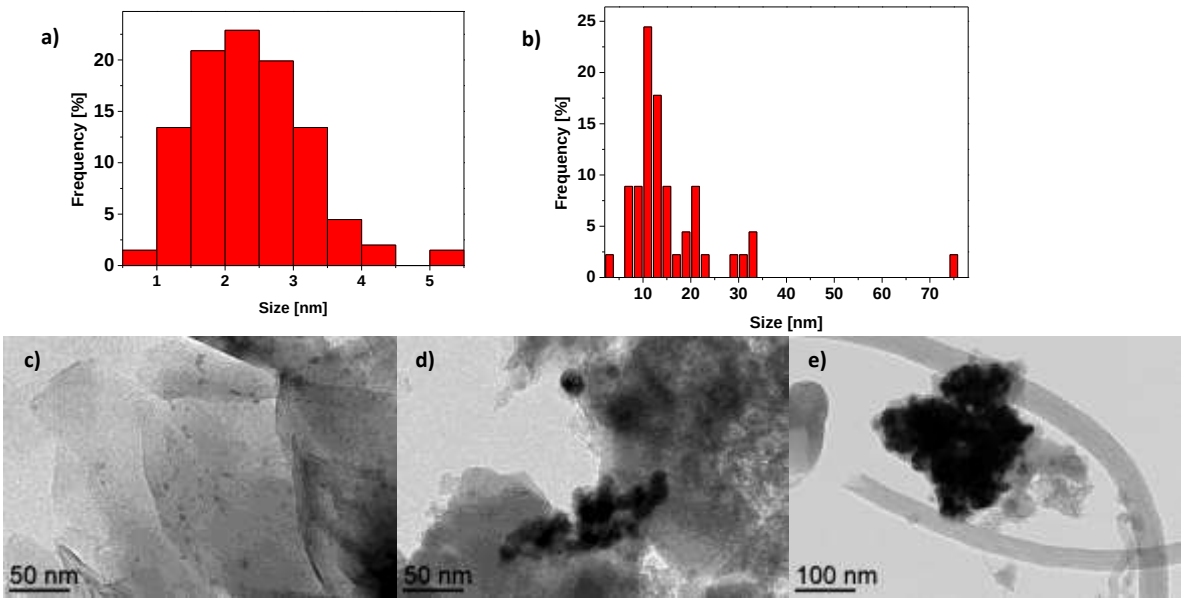

Figure S18. Pd particle size distribution (a, b) and TEM images (c, d, e) for Pd/FLG after three consecutive uses for the vanillin hydrodeoxygenation reaction (a, c) and 5-hydroxymethylfurfural oxidation (b, d, e).